Case Studies in Thermal Engineering 63 (2024) 105313

Contents lists available at ScienceDirect

Case Studies in Thermal Engineering

journal homepage: www.elsevier.com/locate/csite

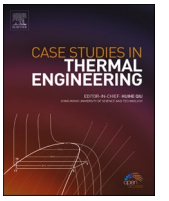

Experimental investigation of heat transfer enhancement, thermal efficiency, and pressure drop in forced convection of magnetic hybrid nanofluid (Fe_3O_4/TiO_2) under varied magnetic field strengths and waveforms

Victor O. Adogbeji [a], Mohsen Sharifpur [a,b,c,*], Josua P. Meyer [a,d]

[a] Department of Mechanical and Aeronautical Engineering, University of Pretoria, Pretoria, Private Bag X20, Hatfield, 0028, South Africa
[b] School of Mechanical, Industrial and Aeronautical Engineering, University of the Witwatersrand, Private Bag 3, Wits, 2050, South Africa
[c] Department of Medical Research, China Medical University Hospital, China Medical University, Taichung, Taiwan
[d] Department of Mechanical and Mechatronic Engineering, Stellenbosch University, Stellenbosch, South Africa

ARTICLE INFO

Keywords:
Varied magnetic field strengths
Waveforms
Hybrid nanofluid
Heat transfer
Convective flow
Thermal efficiency
Pressure drop
Frequency optimization
Nanoparticle concentration
Turbulent forced convection

ABSTRACT

Applying a magnetic field to influence convective flow of ferrofluids has become an efficient method for enhancing heat transfer in thermal systems, particularly in straight tubes. This study investigates the heat transfer properties of Fe_3O_4/TiO_2 nanofluids within a heated copper tube under varied magnetic field strengths and waveforms. Optimal magnetic field conditions were determined at 4 V and 60 Hz across all waveform types, as higher frequencies and voltages increased magnetic field intensity, thereby reducing heat transfer rates. Magnetic waveforms exerted differential influences on pressure drop, indicating varied nanoparticle alignment and turbulence levels, impacting fluid flow dynamics and viscosity. Higher nanoparticle concentration (0.1% vol) correlated with increased pressure drops across sine, square, and triangular waveforms, suggesting heightened flow resistance and potential nanoparticle agglomeration, thus reducing thermal efficiency. Conversely, lower concentrations exhibited enhanced thermal performance due to improved nanoparticle dispersion and reduced thermal resistance. At 0.1% vol, heat transfer enhancement without a magnetic field was 16.5%. The introduction of magnetic field waveforms attenuated this enhancement: 15.3% (sine), 13.26% (square), and 12.59% (triangular). Conversely, at lower volume fractions, heat transfer enhancements with magnetic fields exceeded those without at 0.05% vol, enhancements were 20.92% (sine), 21.3% (square), and 21.34% (triangular); at 0.025% vol, enhancements were 22.07% (sine), 22.3% (square), and 21.32% (triangular); at 0.0125% vol, enhancements were 27.87% (sine), 28.21% (square), and 26.74% (triangular); and at 0.0065% vol, enhancements were 22.24% (sine), 22.3% (square), and 24.49% (triangular).

* Corresponding author. Department of Mechanical and Aeronautical Engineering, University of Pretoria, Pretoria, Private Bag X20, Hatfield, 0028, South Africa.
E-mail address: mohsen.sharifpur@up.ac.za (M. Sharifpur).

https://doi.org/10.1016/j.csite.2024.105313
Received 30 June 2024; Received in revised form 12 October 2024; Accepted 20 October 2024
Available online 22 October 2024

1. Introduction

Over the last decade, nanotechnology has revolutionized heat transfer methods, introducing cutting-edge strategies that enhance thermal efficiency across a broad range of engineering applications. Among these innovations, magnetic hybrid nanofluids suspensions of magnetic nanoparticles in base fluids have emerged as highly promising contenders. These advanced fluids, when subjected to magnetic fields and pulsating parameters, offer a novel and precise approach to controlling and optimizing heat transfer processes in real time.

Forced convection heat transfer plays a critical role in numerous modern industrial systems, where efficient thermal management is paramount. While the impact of magnetic fields (MF) on heat transfer and the use of nanofluids (NF) has been extensively studied, recent advancements have broadened their applicability to diverse fields [1].From electronics cooling [2], solar collectors [3], jet impingement applications [4], photovoltaic panels [5], boiling processes [6], automotive applications [7], heat exchangers [8] circular tubes [9], vapor absorption systems [10], energy-efficient technologies, and material processing [11]. Across these sectors, integrating magnetic nanofluids has consistently driven substantial gains in both thermal efficiency and overall system performance, while also leading to noteworthy energy savings.

This convergence of magnetic fields and nanotechnology marks an exciting frontier in heat transfer optimization, offering untapped potential for future industrial breakthroughs. Tekir et al. [12]conducted an experimental investigation on the convective heat transfer characteristics of Fe_3O_4/H2O nanofluid (with volume fractions ranging from 0.0% to 0.05%) in a straight tube. The study compared the impact of direct current (DC) and alternating AC) magnetic fields under various conditions. Tekir and the team explored different AC magnetic field wave types, including triangle, square and sinus, and varied frequencies (f) from 2 to 15 to determine the optimal wave type and frequency. The findings revealed that using DC magnetic field resulted in a 13% enhancement in convective heat transfer. In comparison, applying AC magnetic fields increased the convective heat transfer rate by up to 35%. Gurdal et al. [13] investigated the forced convection of Fe_3O_4/water flowing through both dimpled and smooth tubes under the influence of an alternating magnetic field (frequency = 5 Hz, and magnetic field strength = 0.16 T with a 1.0% volume fraction in the laminar flow regime). The researchers explored different magnetic field wave types, at various axial distance positions, including triangle, square and sinus (x/D = 60x/D, 20, x/D = 40, and x/D = 20). Their outcome revealed that the highest convective heat transfer ratio was achieved at the x/D = 20 location, particularly with the square wave type for all cases. Specifically, the average *Nu* of the dimpled tube subjected to the square wave type at x/D = 20 showed a notable increase of 58.13%. Abadeh et al. [14]. conducted an experimental investigation into the pressure loss and heat transfer characteristics within a straight tube utilizing Fe_3O_4/water as the working fluid. The study involved exposure to an alternating current magnetic field (ACMF) with frequencies of 1000, 100, 10, and 0 Hz, operating under laminar flow conditions (Re = 535, 1070, 1605, and 2140). The findings revealed that the *Nu* experienced enhancements of 11.85% and 14.8% when subjected to ACMF with frequencies of 10 and 100 Hz, respectively. However, no noticeable increment was observed at frequencies ranging from 100 to 1000 Hz. Sun et al. [15]. conducted an experiment to assess the influence of magnetic fields on CHT in hydromagnetic nanofluids containing Fe_3O_4 nanoparticles. The study revealed that higher magnetic flux density, specifically 415 G, led to a notable 4.36% improvement in heat transfer at a Re of 1080. Additionally, a 700-G magnetic field resulted in a more significant enhancement of 7.19%. Interestingly, a field gradient of 28.6 G/mm induced chain-like structures, contributing to a substantial 32.0% increase in the local Nusselt number. The overall heat transfer enhancement was observed despite increased pressure drop caused by flow disturbance. The experimental investigation covered Re ranging from 400 to 2000 and volumetric fractions of Fe_3O_4 nanoparticles ranging from 0.1% to 0.9%. Zhang and Zhang [16] conducted an experiment to examine the hydraulic effectiveness of Fe_3O_4/water in the presence of an alternating current magnetic field. The experimental results revealed that the overall heat transfer efficiency demonstrated superior effectiveness at lower frequencies (f) and Re. The improvement in heat transfer was ascribed to both the migration and buildup of magnetic nanoparticles (NPs) along the tube's wall induced by the Alternating Current magnetic field and the turbulent flow behavior of the Fe_3O_4/water. Goharkhah et al. [17]. assessed the influence of constant and varying magnetic fields on laminar convective heat transfer (CHT) within a heated tube utilizing a 2% concentration water-based ferrofluid containing Fe_3O_4 nanoparticles. The ferrofluid demonstrated a 13.5% enhancement in convective heat transfer compared to DIW when examined at Re 1200. Furthermore, when subjected to constant and alternating magnetic fields with a density of 500 G, the improvement in heat exchange was notably amplified, reaching 18.9% and 31.4%, respectively. Karamallah et al. [18] in horizontal tube experiments with Fe_3O_4 nanofluid Re 2900–9820, nanoparticle volume fractions 0.3%–0.9%), nanofluid use increased the *Nu* by 5.4%–42.7%. Application of magnetic fields (0.1–0.3 T) further enhanced it to 43.9%–46% at 0.9% volumetric fraction. Heat exchange improvement decreased with higher Re under the magnetic field. Lee et al [19]. studied the impact of a magnetic field on CHT using different nanofluids, ethylene glycol water-based Fe_3O_4 nanofluids, and MWCNT/Fe_3O_4 hybrid nanofluids with Re 1000 to 1600 and nanoparticle volume fractions from 0.025% to 0.2%. They found the highest CHT coefficients in MWCNT nanofluids, with enhancements of 2.78 % and 3.23% for 0.2 wt% Fe_3O_4 and 0.1 wt% Fe_3O_4, respectively. Moreover, they observed increased average pressure drops, with increments of 4.73% and 5.23% for 0.2 wt% Fe_3O_4 and 0.2 wt% Fe_3O_4/MWCNT nanofluids. Shahsavar et al [20]. In the study of Fe_3O_4/CNT hybrid nanofluids, heat exchange improvement of up to 62.7% in the local *Nu* was observed without a magnetic field. The applied constant magnetic field further improved heat exchange, with the optimum improved by 20.5% when evaluated alongside to no magnetic field, influenced by nanoparticle concentrations and Re. Tekir et al. [21] evaluated the impact of a constant magnetic field on CHT in a Fe_3O_4-Cu/water hybrid nanofluid. They explored Re 994 to 2337 and volumetric fraction from 0.02% to 2.0%. Their results revealed that higher flow rates increased the *Nu* and that the nanofluids improved heat exchange in the pipe. Importantly, the applied magnetic field increased CHT by 14% when evaluated alongside to no magnetic field conditions. Shi et al. [22] explored magnetically controlled convective heat transfer using a MCNT with CTNs and Fe_3O_4. They investigated various parameters, including electromagnet spacing (0 – 150 mm), rotation angles (0°, 30°, 60°, 120°), and magnetic field strengths (100 Gs, 200 Gs, 400 Gs, 800

Gs), across Re, 60 to 540 and nanoparticle volumetric fraction of 0.02%–2.0%. Their findings showed that the magnetic field significantly improved heat exchange, with a 12.2% increment in average heat exchange efficiency and a local heat exchange efficiency improvement exceeding 30.2%. Talebi et al. [23] investigated forced convection using nanofluids containing Cu, Fe_3O_4, and Cu/ Fe_3O_4 hybrid nanoparticles at different volume fractions (1% – 4%) and Re (600, 1200, 1800). They found that the presence of these nanoparticles improved the heat exchange efficiency, with a more pronounced effect in the case of the hybrid nanofluid, showing an 11.9% improvement compared to Cu/water nanofluid's 7.8% enhancement. Mehrali et al. [24] investigated graphene-magnetite oxide-Fe_3O_4 hybrid nanofluids for entropy generation and heat transfer under forced convection with a constant magnetic field. Their results showed improved heat transfer when evaluated alongside distilled water, and this improvement was even more significant when a magnetic field was applied. Additionally, they observed a substantial 41% reduction in the rate of entropy generation in comparison to distilled water. Shyam et al. [25] investigated Re 66 to observe heat transfer enhancement using ferrofluid (volume fraction $\varphi = 4.64\%$) flow in a straight tube. They applied AC magnetic fields with frequencies ranging from 1 Hz to 5 Hz and DC magnetic fields with strengths of 0 Gauss (G), 700G, and 1080G. The findings indicated that using AC magnetic fields led to a substantial increase of 39% in the convective heat transfer rate.

Existing research on CHT has predominantly focused on single nanofluids, particularly those incorporating Fe_3O_4 nanoparticles, with extensive studies documenting the behavior of these nanofluids in laminar flow regimes and their interactions with magnetic fields. However, there is a noticeable scarcity of research on hybrid nanofluids, such as Fe_3O_4 combined with Ti O_2, in turbulent flow regimes. Additionally, while previous studies have explored heat transfer in laminar conditions, they largely overlook the impact of magnetic waveform variations and pulsating parameters on heat transfer and pressure drop in more complex turbulent flows.

This study aims to fill this gap through a comprehensive experimental investigation into the influence of magnetic field strength and pulsating parameters on heat transfer and pressure drop in turbulent forced convection, using magnetic hybrid Fe_3O_4/Ti O_2 nanofluids. By systematically varying waveform types (sine wave, square wave, triangular wave), voltages (2 V, 4 V, 6 V, 8 V, 12 V), frequencies (40 Hz, 60 Hz, 100 Hz, 500 Hz, 1000 Hz), and volume fractions (0.1%, 0.05%, 0.025%, 0.0125%, 0.00625%), this study not only addresses a critical gap in the literature but also introduces several key innovations.

Key innovations include the identification of optimal magnetic field conditions (4 V and 60 Hz across all waveform types), a novel analysis of how waveform variations and magnetic field strengths impact nanoparticle alignment, fluid flow dynamics, and pressure drop. The study also provides new insights into the correlation between nanoparticle concentration and thermal efficiency, demonstrating that lower nanoparticle concentrations enhance heat transfer performance, while higher concentrations increase pressure drop. These findings challenge existing paradigms and present opportunities for optimizing thermal systems using magnetic hybrid nanofluids in turbulent regimes.

2. Experimental setup and procedure

2.1. Preparation and characterization of MHNFs

In the experimental setup, magnetic nanoparticles were composed of iron (III) oxide (Fe_3O_4) (20–30 nm) and a purity level of 95.5%. Additionally, titanium dioxide (Ti O_2) with an 18 nm diameter and a purity of 99.9% was employed, adhering to the manufacturer's specifications for particle size. The TiO_2 nanoparticles were procured from Nanostructured and Amorphous Materials Inc. in Houston, Texas, USA, while the remaining materials were obtained from US Research Nanomaterial Inc., also in Houston, Texas, USA. To enhance the stability of the hybrid nanofluids (MHNFs), Gum Arabic (GA), with a purity of $\geq$98.5%, sourced from Sigma-Aldrich in Berlin, Germany, was utilized as a surfactant. Table 1 provides the thermal properties of both the base fluid and nanoparticles utilized in the study, with material characteristics and parameters obtained from the product datasheets provided by the respective companies.

The synthesis of MHNFs involved a two-step process, where Fe_3O_4 and Ti O_2 were mixed at an 80 %–20% ratio, respectively, using a digital weighing balance (Radwag AS 220.R2, Radom, Poland, with an accuracy of $\pm$0.01 g). Gum Arabic acted as a surfactant at a weight ratio of 0.75 to ensure MHNF stability. The resulting stable MHNFs, comprising Fe_3O_4 and Ti O_2 nanoparticles were quantified using Equation (1) [26] and prepared by dispersing the nanoparticles in DIW through ultrasonication with a Qsonica Q-700 ultrasonicator. Ultrasonication lasted for 4 h, utilizing a programmed sequence of 5-s pulses with 2-s intervals to maintain stability. This consistent approach applied to all MHNFs, maintaining volume concentrations at 0.1%, 0.05%, 0.025%, 0.0125%, and 0.00625% at a constant temperature of 20 °C. To ensure the desired temperature during sonication and thermophysical assessments, a programmable water bath (LAUDA ECO RE1225, Berlin, Germany) with precise temperature control was utilized.

Table 1
Thermal characteristics of investigated materials at standard room temperature.

Properties	Deionized water (DIW)	Iron (III) oxide (20–30 nm)	Titanium dioxide (18 nm)
Density (kg/m^3)	997	4950	4175
Thermal conductivity (W/m.k)	0.613	80.4	8.4
Specific Heat capacity (J/kg.k)	4179	670	692
Shape	–	Plate-like nanosheet	spherical

$$\varphi = \left(\frac{Y_{Fe_3O_4} \left(\frac{W}{\rho}\right)_{Fe_3O_4} + Y_{TiO_2} \left(\frac{W}{\rho}\right)_{TiO_2}}{Y_{Fe_3O_4} \left(\frac{W}{\rho}\right)_{Fe_3O_4} + Y_{TiO_2} \left(\frac{W}{\rho}\right)_{TiO_2} + \left(\frac{W}{\rho}\right)_{DIW}} \right) \quad (1)$$

A variety of equipment was utilized for different purposes throughout the study. These instruments comprised a pH meter (Jenway 3510, Staffordshire, UK) with a range of −2 to 19.999 and an accuracy of ±0.003, a vibro-viscometer (SV-10A series, A&D, Tokyo, Japan) with an accuracy of ±1%, a UV–visible spectrophotometer (Jenway, Staffordshire, UK), a transmission electron microscope (JEOL JEM-2100F, Tokyo, Japan) for examining dry samples, and a conductivity meter (CHAUVIN ARNOUX, C.A 10141 Instrument, France) with an accuracy of ±1%. These instruments played various roles in facilitating thorough analysis and accurate measurements throughout the research. Furthermore, the prepared MHNFs underwent characterization for thermal conductivity (κ) and viscosity (μ) across a range of temperatures, spanning from 10 °C to 50 °C. This analysis was conducted using the KD2 Pro (Decagon Devices Inc). Thermal Properties Analyzer (METER Group) with an accuracy of ±10% for κ within the 0.02–2.0 W/m/K range, enabling the assessment of MHNF thermal properties under varying temperature conditions. These techniques and instruments were employed to comprehensively evaluate the stability, thermophysical properties, and other characteristics of MHNFs, ensuring precision and reliability. For instance, transmission electron microscopy (TEM) was employed to scrutinize the morphology and distribution of MHNFs, while stability monitoring involved multiple methods such as viscosity measurements, UV–visible spectrophotometry, thermal conductivity measurements, and visual inspections, as shown in Fig. 1.

To ascertain the stability of the MHNFs nanofluids, at least one of these properties needed to remain constant throughout the stability evaluation period. In our investigation, we carried out a thorough analysis, incorporating UV–visible spectrophotometry, thermal conductivity measurements, and viscosity techniques. These evaluations were conducted immediately after sonication for 24 h and covered a spectrum of temperatures from 10 °C to 50 °C. Moreover, visual inspections were performed on a weekly basis over the span of one month.

2.2. Description of magnetic equipment configuration for enhanced heat transfer

The instrumentation for magnetic field-induced heat transfer enhancement in magnetic hybrid nanofluids involves a comprehensive set of equipment and tools. Key components include a Digital Storage Oscilloscope (IDS-2000A series), UNI-T UT900E series Function generator (Waveform generator), Accel Instruments TS250 Waveform Amplifier, electromagnets (220L × 46W × 29D), gaussmeter GM08 for measuring the magnetic field, and a distribution box for controlled connectivity. The electromagnets, operating with dual voltage options (12 V and 24VDC) and a current draw of up to 250 mA, are connected in parallel to the waveform amplifier, which serves as the main power source. The oscilloscope, linked to the output of the waveform amplifier, monitors waveform current and voltage. The waveform generator facilitates frequency, period, and duty cycle adjustment, and is connected to the waveform amplifier's input. The output from the Waveform Amplifier connects to a distribution box, allowing individual control of four electromagnets, whilst the function generator adjusts magnetic field pulsation via generated sine, square, and triangular waves of user-selectable amplitudes and frequencies. Current and voltage waveforms are displayed on the oscilloscope screen. The four electromagnets are positioned strategically on top of the test section and enable coverage of all seven thermocouples stations, as shown in Fig. 2. Initial magnetic field measurements involve varying the parameters, including waveform variations (sine wave, square wave, triangular wave), voltages are presented in Table 2. The system is allowed to reach a steady state before applying the magnetic field, which is done simultaneously with continuous heat flux.

2.3. UV–visible spectrophotometry

The UV–Vis spectroscopy analysis of MHNFs was conducted using an ONDA TOUCH UV-21 Spectrophotometer at room temperature, with DIW serving as the reference standard. Each measurement was performed six times, and the averages were calculated. The spectral range of the light-covered wavelengths is from 200 to 300 nm, with intervals of 10 nm from 200 to 280 nm and 1 nm intervals from 281 to 300 nm for all samples. The absorbance of MHNFs at various wavelengths and sedimentation percentage were determined using Equation (2).

$$\text{Percentage (SF)} = \left(\frac{\textit{Sedimentation factor}}{\text{Initial Absorbance}} \right) \quad (2)$$

Fig. 1. Visual Inspection of different concentrations of Fe_3O_4/Ti O_2/DIW **Magnetic hybrid nanofluid**.

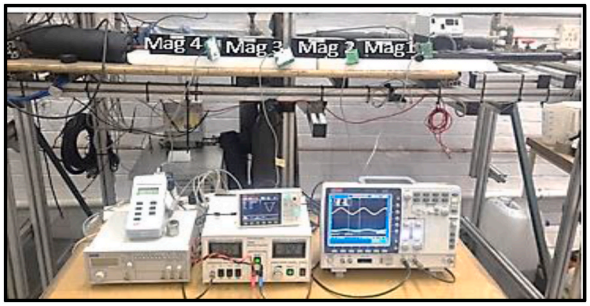

Fig. 2. Experimental setup and pulsating parameter control.

Table 2
Variation of magnetic field parameters and measurement.

Waveforms	Voltage (V)	Duty cycle	Frequency (Hz)	Periods (Ms)	Phase
Sine	2	50 %	40	16.67	90°
Square	4		60	12.5	
Triangular	6		80	10.0	
	8		100	2.0	
	12		500		
			1000		

2.4. Experimental setup for measuring thermal, electrical conductivity and pH

This study's experimental configuration for measuring thermal conductivity consisted of two primary components: the apparatus for thermal conductivity measurement and the constant temperature bath. A programmable water bath was employed to ensure precise temperature control. Thermal conductivity measurements were conducted continuously over 24 h, spanning a temperature range from 10 °C to 50 °C at 5 °C intervals. The KD2 pro instrument manufactured by Decagon Devices Inc. was used to determine the thermal conductivity of MHNFs. This instrument operates within the specified range of 0.02 W·m−1·K−1 to 2 W·m−1·K−1, with a manufacturer-stated uncertainty level of 5%. Accurate readings necessitate maintaining a minimum of 15 mm of the material being measured parallel to the sensor in all directions, as the sensor emits a heat pulse. The fluid's electrical and pH were also determined with variations in temperature from 10 °C to 50 °C at 5 °C intervals, as depicted in Fig. 3b.

2.5. Viscosity measurement

Viscosity, a crucial thermophysical property for assessing nanofluid stability, was measured for MHNFs (Fe_3O_4/Ti O_2/ DI Water) across a temperature range from 10 °C to 50 °C in this research. The vibro-viscometer was calibrated to ensure measurement accuracy before conducting viscosity measurements. For consistent temperature conditions during the experiment, the vibro-viscometer jacket was connected to a programmable water bath (LAUDA, Berlin, Germany, model ECO RE1225) and a data logger, as depicted in Fig. 3a. The temperature of MHNFs was adjusted between 10 °C and 50 °C in 5 °C increments. Initial viscosity measurements were taken immediately after nanofluid preparation, and continuous monitoring over 24 h assessed the stability of each volume fraction. This comprehensive approach allowed for evaluating MHNF viscosity under varying temperatures and over different time intervals.

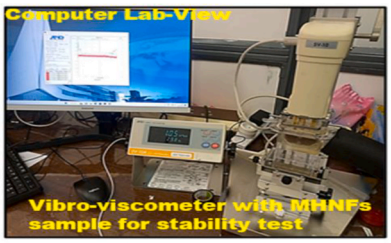

Fig 3: (a) Determination of viscosity (b) Determination of electrical conductivity and pH.

Fig. 3. (a) Determination of viscosity (b) Determination of electrical conductivity and pH.

2.6. Experimental setup for forced convective heat transfer and methodology

Fig. 4a and b illustrate the experimental setup and the layout of the test rig, encompassing components such as a tube-in-tube heat exchanger, a flow meter, a DC power supply, a micro gear pump, a test section, a storage tank, thermocouples, a pressure transducer, and a data acquisition system. This configuration is tailored to investigate nanofluid heat transfer characteristics. The test section is equipped with a Constantine heating wire wound around it to provide controlled heat, and efficient insulation is integrated to minimize heat dissipation. Nanofluids with varying weight concentrations are pumped through a copper pipe, and their mass flow rate is precisely measured using a flow meter. Maintaining a constant inlet temperature of 20 °C, the heated nanofluids are cooled through a heat exchanger, transferring heat to cold water facilitated by a circulation pump. The data acquisition system collects and processes signals from various sensors, including flow meters, pressure transducers, thermocouples, and the power supply.

In Fig. 4c, the testing segment showcases a circular copper tube, 1550 mm in length, with an inner diameter of 8 mm and an outer

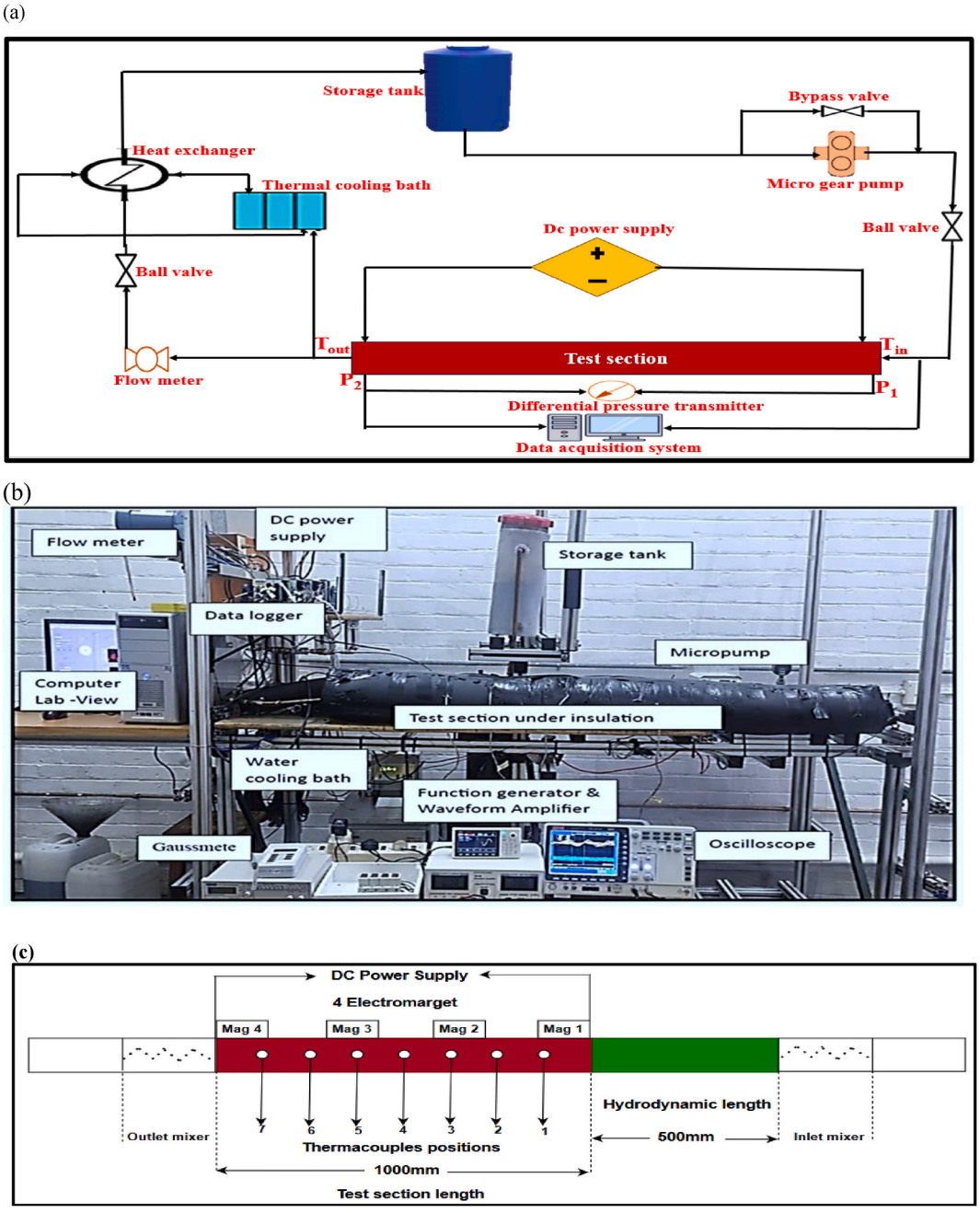

Fig. 4. (a) Experimental configuration schematic (b) Overview of test rig components (c) Experimental test section Configuration.

diameter of 9.5 mm. Four strategically positioned thermocouples monitor tube wall temperatures at regular 130 mm intervals in the North, South, East, and West directions. Continuous temperature monitoring occurs at both the nanofluid inlet and outlet. A 200 W Constantine wire ensures a consistent heat flux, powered by a DC source supplying 1.22 A and 180 V. The shorter test section of 1000 mm length ensures fully developed hydraulics, and four strategically positioned electromagnetic lock blocks on the test tube enable coverage of all seven thermocouples. Experiments are conducted three times to ensure data accuracy, and calculations are based on the average wall temperature.

The thermophysical properties of the MHNFs were assessed, and the density, as well as the specific heat of each MHNF, were determined using Pak and Cho's analytical model [27], as represented in Equations (2) and (3).

$$\rho_{nf} = (1-\varphi)\rho_{bf} + \varphi\rho_{np} \tag{3}$$

$$c_{nf} = (1-\varphi)c_{bf} + \varphi c_p \tag{4}$$

$$\rho_{pnf} = \frac{(1+\varphi)\rho_{bf}C_{pbf} + \varphi\rho_{np}C_{pnp}}{(1-\varphi)\rho_{bf} + \varphi\rho_{np}} \tag{5}$$

$$C_{pnf} = \frac{(1+\varphi)C_{bf}C_{pbf} + \varphi\rho_{np}C_{pnp}}{(1-\varphi)\rho_{bf} + \varphi\rho_{np}} \tag{6}$$

In these equations, φ represents the mass ratio of NF, while ρ_{nf}, ρ_{bf}, and $\varphi\rho_{np}$ and $\varphi\rho_{np}$ refer to the densities of the nanofluid, base fluid, and nanoparticles, respectively. Furthermore, C_{pnf}, C_{pbf}, and C_{pnp} indicate their respective specific heats. The specific heat and density determination for MHNFs containing Fe_3O_4/Ti O_2 is carried out through the application of Equations (5) and (6) [28].

The examination of CHT and Nusselt number at different volume fractions requires the use of thermophysical properties. To be more specific, this involves calculating the heat absorbed by the working fluid and the energy delivered to the test section, as outlined in Equations (7) and (8) [28].

$$P = VI \tag{7}$$

$$Q = \dot{m}c(T_O - T_i) \tag{8}$$

In the equation, V denotes voltage, I refers to the current supplied by the power source, m and c represent the mass flow rate and specific heat of the working fluid, respectively. T_O *and* T_i correspond to the outlet and inlet temperatures of the test section, respectively. Employing Equation (9) [8], calculations are performed to determine the local CHT coefficient along the axial distance of the test section.

$$h = \frac{Q}{A(t_w - t_b)} \tag{9}$$

To determine the local CHT coefficient at each thermocouple point, the bulk fluid temperature was calculated by using the inlet and outlet temperatures, specific heat, and heat flux data obtained from a flow meter. This information was then compared with the surface temperature recorded by the thermocouples, enabling the computation of the *Nu*. The *Nu* was derived using the obtained CHT coefficient from Equation (10) [8] and the measured thermal conductivity of the nanofluid.

$$Nu = \frac{hD_i}{k} \tag{10}$$

Where A denotes the test section's area, t_w represents the average wall temperature, t_b stands for the average bulk temperature, and *Nu* is directly related to the CHT. Here, D_i represents the inlet diameter of the test section, and K corresponds to the thermal conductivity of the nanofluids.

In addition to conducting heat transfer measurements, the study also involved evaluating viscous pressure losses in the test section for both deionized water and nanofluids. The obtained experimental results were then compared with projected pressure loss estimates in Equation (11) [29].

Table 3
Experimental conditions and parameters used.

Parameters	Dimensional values/Ranges	Symbols
Reynold Numbers	1000–8000	Re
Heat flux	8.67kw/ m^2	$\dot{q}$
External diameter	9.5 mm	D_O
Internal diameter	8 mm	D_I
Test section length	1000 mm	L
MHNFs inlet temperature	21 °C	T_i

$$f = \frac{\Delta P}{\left(\frac{L}{D_i}\right)\left(\frac{\rho v^2}{2}\right)} \tag{11}$$

Before exploring convective heat transfer coefficients with nanofluids, we ensured the reliability of our experimental setup by conducting tests with Deionized Water (DIW) in a circular tube within the Reynolds number range of 3200–55000. We validated our findings by comparing them to the equations proposed by Ghajar and Tam (1994) [30] and Olivier and Meyer [31], specifically designed for turbulent flows, as expressed in Equations (12) and (13) and Table 3 shows the experimental conditions and parameters used.

$$\mathrm{Nu} = 0.026.\, Re^{0.8}.Pr^{0.385}.\left(\frac{x}{D}\right)^{-0.0054}\left(\frac{u}{u_w}\right)^{0.4} \tag{12}$$

$$3 \le \frac{x}{D} \le 192; 7000 \le 49000; 4 \le Pr \le 34; 1.1 \le \frac{u}{u_w} \le 1.7$$

$$\mathrm{Nu} = 0.026.\, Re^{0.788}.Pr^{\frac{1}{3}}.\left(\frac{u_b}{u_w}\right)^{0.4} \tag{13}$$

With the range of 3.73 ≤ Pr ≤ 5.06 and 3000 ≤ Re ≤ 17800.

Fig. 5 compares the current experimental Nusselt numbers with the correlations developed by Olivier and Meyer, showing an average deviation of 0.47 % (maximum 6.6 %) in turbulent flow conditions. Similarly, Ghajar and Tam's correlation exhibits an average deviation of 3.4 % (maximum 10.5 %) in turbulent flow conditions. These results closely align with the experimental findings using DI water.

2.7. Data reduction and uncertainty

The methodology outlined by Dunn [32], was utilized to quantify the uncertainties pertaining to both the measured and evaluated parameters. These uncertainties were rigorously evaluated at a 95 % confidence level, as demonstrated by Equation (14). This approach enabled a comprehensive assessment of the reliability and accuracy of the obtained results, ensuring robustness in the experimental finding

$$su_x = \sqrt{u_B^2 + U_P^2}, P\% \tag{14}$$

where u_B represents bias error and u_p represents precision error in x with a probability of P%.

The determination of parameter uncertainty utilizing measured variables can be achieved through a sequence of equations, as elucidated below in Equations (15)–(17).

$$\mathrm{R}\,(x) = f\left(x_1, x_2, x_{3,} \ldots\ldots\ldots x_n\right) \tag{15}$$

For a given variable x_i, the uncertainty in the parameter R, with respect to both its mean value $\overline{R}$ and its true (actual) value R_{actual}, can be expressed as follows.,

$$R_{actual} = \overline{R} + \delta R \tag{16}$$

where δR is the uncertainty in R can be expressed as follows,

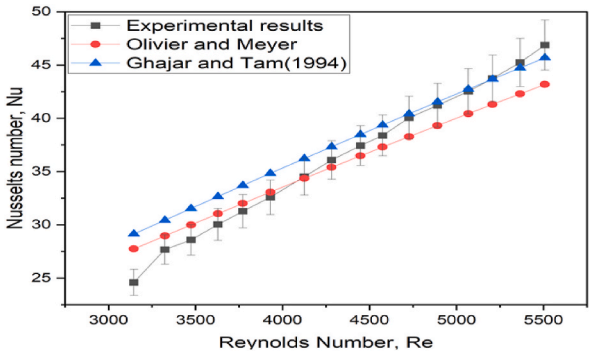

Fig. 5. Validation of experimental setup through Di water testing.

$$\delta R = \sqrt{\left(\delta_{x1}\ \frac{\partial R}{\partial_{x1}}\right)^2 + \left(\delta_{x2}\ \frac{\partial R}{\partial_{x2}}\right)^2 + \ldots\ldots\ldots + \left(\delta_{x_n}\ \frac{\partial R}{\partial_{x_n}}\right)^2} \quad (17)$$

Where x_i represent the uncertainty of the evaluated variable x_i

The uncertainty of the convective heat transfer coefficient (CHT) in the experimental results was determined to be approximately 0.116 %. Table 4 presents the broadest range of uncertainties associated with each parameter across all conducted experiments.

3. Results and discussion

3.1. Nanoparticle morphology analysis in MHFs

The investigation into nanofluids containing Fe_3O_4 and varying ratios of Ti O_2 involved a comprehensive analysis of their morphology and stability using Scanning Electron Microscopy (SEM) imaging. The morphological attributes of Fe_3O_4 and Ti O_2 (18 nm) nanoparticles were meticulously examined through Scanning Electron Microscopy (SEM) imaging, as depicted in Fig. 6. These images were captured at a magnification of 100,000X, employing an accelerating voltage (EHT) of 2.0 kV, and a scanning speed of 9 μm/s. In the SEM image of Fe3O4, a heterogeneous mixture of small and large dispersed plate-like nanosheets was observed. Meanwhile, the SEM image of Ti O_2 (18 nm) nanoparticles revealed spherical shapes. Notably, the SEM image of Fe_3O_4/Ti O_2 exhibited successful nanoparticle suspension, indicating the formation of a stable nanofluid. Furthermore, in the SEM image, Fe_3O_4 nanoparticles appeared more distinct compared to Ti O_2 nanoparticles.

3.2. Exploring thermo-physical characteristics and convective heat exchange of magnetic hybrid nanofluids

To evaluate the stability of the nanofluids, a methodology akin to previous research by Giwa et al. [33], and Osman et al. [34]. was implemented. Utilizing a data logger integrated with a viscosity meter, data was recorded at 5-min intervals over a duration of 10 h, as depicted in Fig. 7a, to assess stability at a temperature of 30 °C. Concurrently, visual inspections were conducted over a 30-day monitoring period. During this period, no sedimentation was observed for nanofluids with volumetric fractions of 0.00625 %, 0.0125 %, and 0.025 %, while slight settling was evident for the 0.05 % volume fraction. Conversely, nanofluids with volumetric fractions 0.1 % displayed signs of settling. These observations align with findings reported by Krishnan et al. [35] UV–Vis spectroscopy, following Beer-Lambert's law [36,37] demonstrated a direct relationship between the absorption rate in Fe_3O_4/Ti O_2 nanofluids and particle volumetric fraction, as depicted in Fig. 7b. The UV–Vis spectroscopy results revealed that lower absorption rates corresponded to decreased particle volumetric fractions, which, in turn, correlated with sedimentation percentages. Over the 30-day period, substantial settling was observed for nanofluids with volume fractions of 0.1 %, with sedimentation factor (SF) percentages of 344.44 %. In contrast, nanofluids with volume fractions of 0.00625 %, 0.0125 %, and 0.025 % exhibited remarkable stability, with SF percentages of 266.68 %, 292.00 %, and 304.72 %, respectively, underscoring their commendable stability. The slight stability observed for the 0.05 % volume fraction suggests the necessity for optimization and stabilizers, particularly at higher concentrations.

Fig. 8a illustrates the viscosity of the MHNFs across temperatures ranging from 10 °C to 50 °C, compared to the viscosity of DIW. A decrease in viscosity is observed with increasing temperature. These findings are consistent with previous studies by Oraon et al. [38] and Zadkhast et al. [39]. However, it is noteworthy that both thermal and electrical conductivity increase as the volume fraction of nanofluids rises. These trends align with the results reported by Giwa et al. [33] and Krishnan et al. [35] as depicted in Fig. 8b and c. Additionally, Fig. 8d demonstrates a decline in the pH levels of nanofluids as temperature rises. Higher nanoparticle concentrations exacerbate this reduction in pH, indicating heightened acidity. This stands in contrast to DIW, which maintains a relatively constant pH of around 7, underscoring the substantial influence of nanoparticles on fluid pH. These observations align with previous studies conducted by Giwa et al. [33] and Krishnan et al. [35], highlighting the intricate interplay between temperature, concentration, and nanofluid characteristics.

Furthermore, Fig. 8e illustrates the effect of varying volume fractions on heat transfer at different Reynolds numbers with Fe_3O_4/Ti O_2 nanofluid. The percentage enhancements in the convective heat transfer (CHT) coefficient for different volume fractions of Fe_3O_4/Ti O_2 nanofluid, in comparison to DIW, exhibit a discernible trend. At 0.1% volume fraction the enhancement is 16%, the enhancement continues to increase with decreasing volume fractions, peaking at about 20.36 at 0.05% volume fraction. Lower concentrations demonstrate more pronounced enhancements, with approximately 21.91% at 0.025% volume fraction and a peak of around 27.28% at 0.0125% volume fraction. Even at 0.00625% volume fraction, there is a notable increase of approximately 22.47% in the CHT coefficient. These results underscore the substantial improvements in CHT coefficient achieved with Fe_3O_4/Ti O_2 nanofluid compared to DIW across various volume fractions.

Table 4
The measured uncertainties in the parameters.

Parameter	Uncertainty (%)
Reynolds number	2.145
Bulk temperature	0.727
CHT coefficient, h	2.49
Nusselt number	3.69

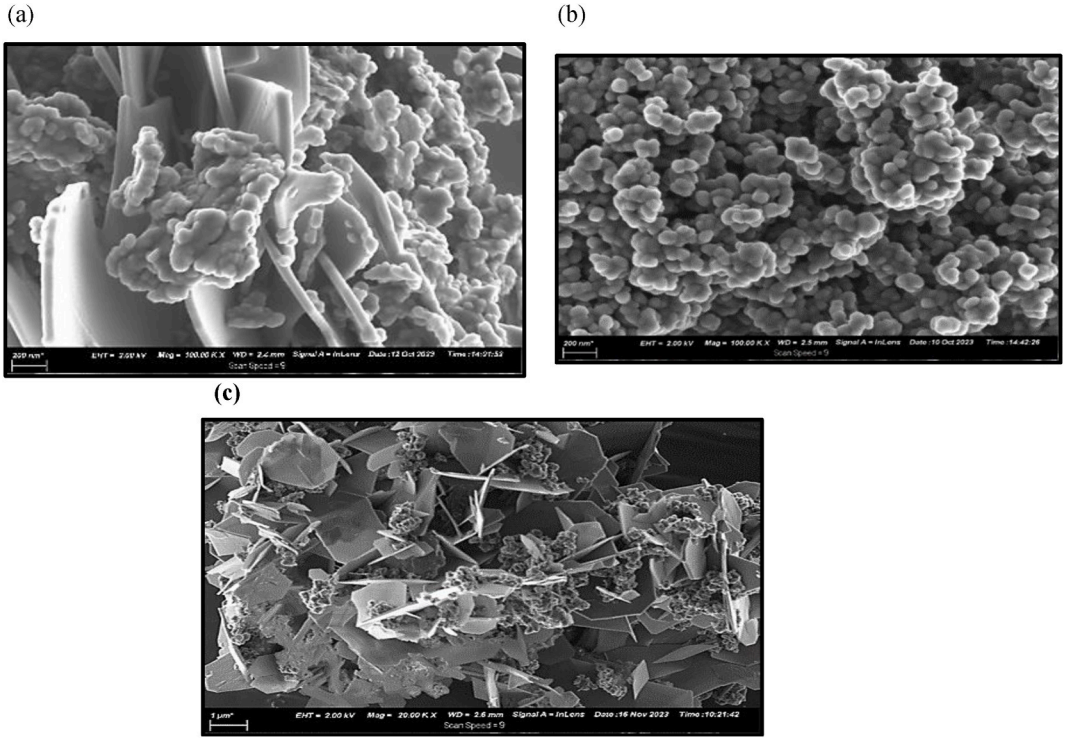

Fig. 6. SEM Analysis of nanoparticle morphology: (a) Fe_3O_4 (20–30nm), (b) Ti O_2 (18 nm) nanoparticles, and (c) Fe_3O_4/Ti O_2 hybrid configuration.

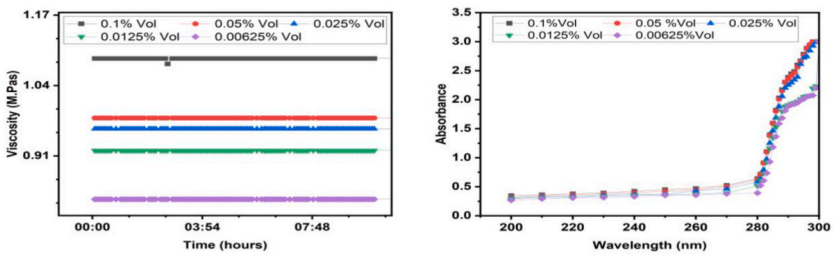

Fig. 7. (a) Time-dependent assessment of stability (b) Influence of Fe_3O_4/Ti O_2 density on light absorption across various wavelengths.

In summary, these findings highlight the significant enhancements in CHT coefficient offered by Fe_3O_4/Ti O_2 nanofluid at different volume fractions compared to DIW. Contrary to conventional beliefs suggesting that higher nanoparticle concentrations lead to improved heat transfer, the data consistently shows that lower nanoparticle concentrations are more effective in this specific nanofluid and flow regime. Possible explanations include improved nanoparticle dispersion, reduced viscosity, and better alignment with flow characteristics at lower concentrations.

Fig. 9a elucidates the intricate relationship between frequency and total magnetic field strength across diverse wave configurations, namely Sine wave, Square wave, and Triangular wave. As the frequency progressively increases from 40 Hz to 1000 Hz, a discernible pattern emerges, depicting a consistent escalation in the total magnetic field strength. The enhancement values, serving as indicators of the magnetic field's impact on heat transfer, consistently climb with higher frequencies for all three waveforms. This observed trend implies a direct and positive correlation between frequency and total magnetic field strength, signifying those heightened frequencies contribute to amplified magnetic field effects on heat transfer. The distinctive performance of each waveform at different frequencies emphasizes the role of wave configuration in influencing this correlation, with the Sine wave consistently exhibiting superior magnetic field effects compared to Square and Triangular waves.

Of note is the convergence point observed at an average of 6.0 and 17.11 T at 40 Hz and 60 Hz, respectively, where all three waveforms intersect. This discovery holds critical implications for optimizing magnetic field conditions, especially in comprehending the impact of magnetic field strength on heat transfer enhancement within the tube at this convergence point. The enhancement of the fluid at this juncture becomes pivotal in determining the optimum frequency required for enhancing heat transfer, thereby influencing the overall efficiency of the heat transfer process. This valuable insight contributes to the broader understanding of the interplay between frequency, magnetic field strength, and heat transfer enhancement, offering potential avenues for optimizing thermal

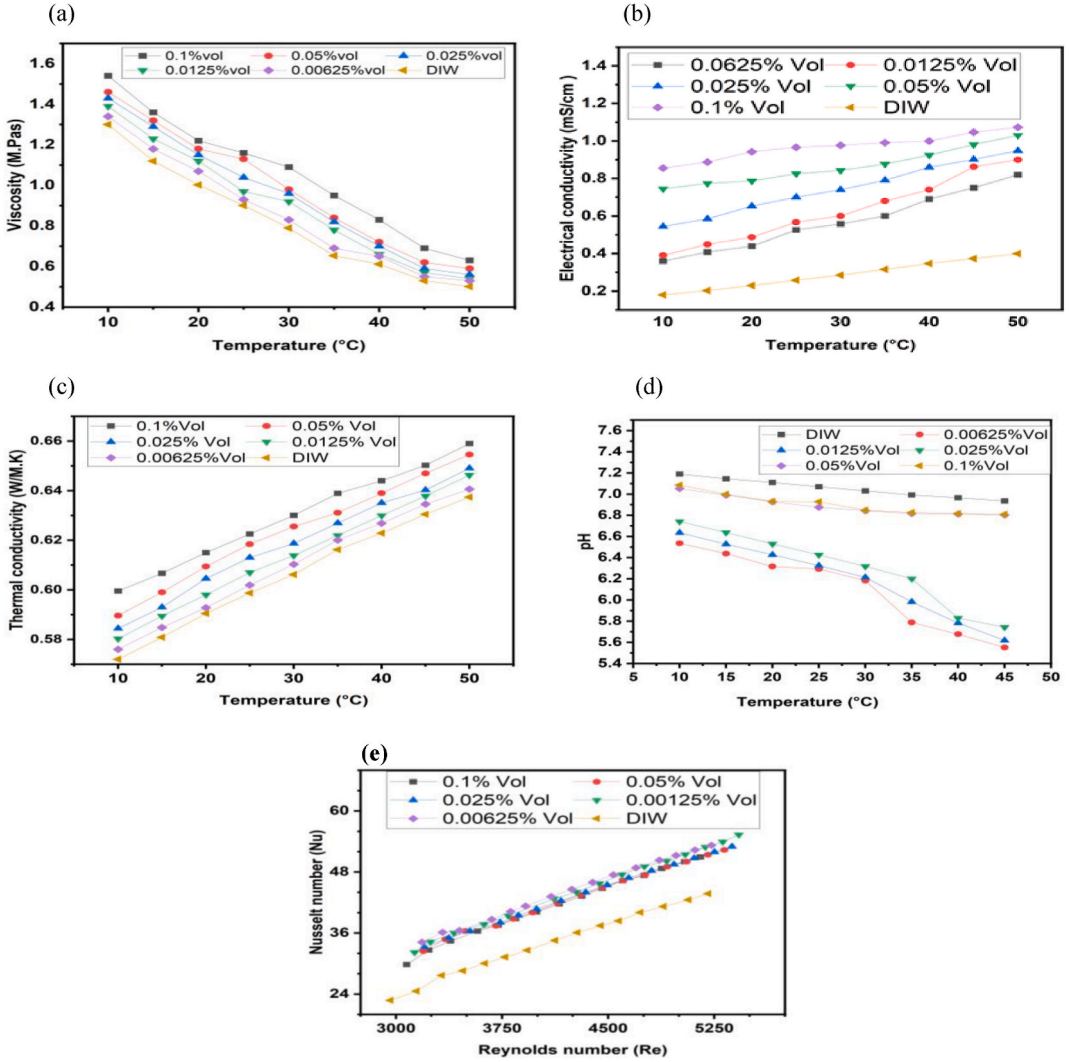

Fig. 8. (a) Effect of various volume fractions on temperature-dependent variation in electrical conductivity
(b) Effect of various volume fractions on temperature-dependent variation in electrical conductivity
(c) Effect of various volume fractions on temperature-dependent variation in thermal conductivity
(d) Effect of various volume fractions on temperature-dependent variation in pH (e) Effect of volume fraction variation on heat transfer across Reynolds numbers.

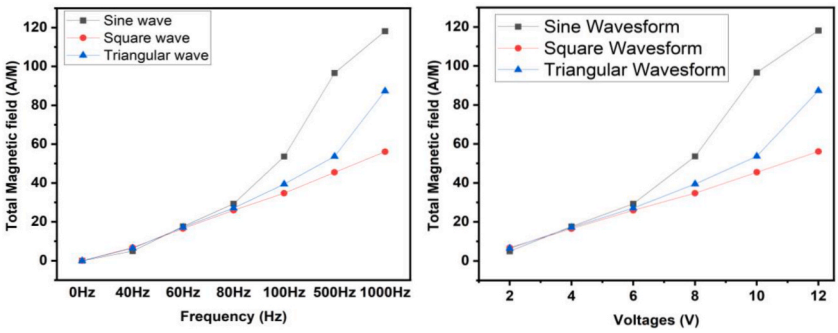

Fig. 9. (a) Optimization of magnetic field strength across various waveforms at different frequency
(b) Optimization of magnetic field strength across various waveforms at different voltage.

processes influenced by varying magnetic fields at different frequencies.

The relationship between voltage and total magnetic field strength is illustrated in Fig. 9b, demonstrating a consistent increase in magnetic field strength as voltage varies from 2 V to 12 V across different waveform types (Sine, Square, Triangular). The total magnetic field represents the cumulative magnetic field strength produced by the three electromagnets, as depicted in Fig. 10, The observed pattern indicates a direct proportionality between voltage and magnetic field strength as depicted in Fig. 9b. Notably, the Sine waveform consistently generates the highest magnetic field strengths compared to Square and Triangular waveforms at each voltage level. The Triangular waveform exhibits intermediate magnetic field strengths, while the square waveform consistently yields the lowest magnetic field strengths. Interestingly, at an average of 17.11 T at 4 V, there is a point of convergence where all three waveforms intersect.

3.3. *Optimization of magnetic field parameters for enhanced heat transfer in hybrid magnetic fluids*

This finding is crucial for optimizing magnetic field conditions, particularly in understanding the impact of magnetic field strength on heat transfer enhancement within the tube. The direct correlation between voltage and magnetic field strength underscores the controllability of the magnetic field, enabling precise adjustments to achieve desired heat transfer outcomes. Additionally, the distinct behavior of different waveform types offers a nuanced understanding of how the shape of the magnetic field waveform influences the overall magnetic field strength. Such insights are essential for designing and implementing efficient thermal management systems that leverage magnetic field-induced heat transfer enhancements.

The data from Fig. 11a and b, and c indicates that at varying voltage settings (4 V, 6 V, 8 V, 12 V) with three magnetic fields on the test section at the thermally developed area of the tube, as shown in Fig. 10, the magnetic field's optimization occurs at a frequency of 60 Hz for different waveforms, including sine, square, and triangular waves. Across various Re, the 60 Hz frequency consistently shows favorable heat transfer characteristics compared to other frequencies, as shown in Fig. 12a and b, c (40 Hz, 80 Hz, 100 Hz, 500 Hz, and 1 kHz) at 4 V for all waveform configurations. This favorable trend persists across diverse Re, highlighting the efficacy of the 4 V magnetic field in improving overall thermal performance.

The optimization observed at 4 V suggests that this specific combination of voltage and frequency is well-suited for maximizing heat transfer within the given system. However, as the voltage increases from 6 V to 12 V, the magnetic field strength also increases, reducing heat transfer. These observed trends align with the conclusions drawn by Abadeh et al. [14], Azizian et al. [40] and Zhang and Zhang [16], but are in contrast to the findings reported by Sun et al. [15] and Hatami at el [41]. This trend is consistent across all waveforms, indicating that the fluid's magnetic properties tend to adhere to the surface of the tube as the fluid flows along it. In contrast, at 4 V, the magnetic properties of the fluid are effectively suspended within the fluid, thereby enhancing heat transfer.

For instance, at Re 5423.12, the 60 Hz Sine wave at 4 V exhibits a higher value (55.03) than other frequencies, indicating enhanced heat transfer. This trend holds across different Re, highlighting the effectiveness of the 60 Hz frequency in improving thermal performance at 4 V for all waveform types, and sine wave appears to be the best among the waves considered, as shown in Figure. The observed optimization at 60 Hz suggests that this specific combination of voltage and frequency is well-suited for maximizing heat transfer in the given system, potentially indicating a resonance or resonance-like behavior in the magnetic field's impact on thermal performance. Notably, the heat transfer enhancement may vary at other voltages (6 V, 8 V, 12 V), and the 60 Hz frequency still appears to be a favorable choice.

The diminishing heat transfer at higher frequencies could be attributed to the changing magnetic properties or interactions within the fluid at different frequencies, affecting the suspension of magnetic particles and, consequently, heat transfer efficiency. Further analysis and exploration of the underlying mechanisms driving this frequency-dependent behavior would provide valuable insights into optimizing the magnetic field for enhanced heat transfer in the given system. Consequently, for any magnetic fluid subjected to a magnetic field using an electromagnet, it becomes crucial to determine the optimum voltage and frequency to achieve improved enhancement. The findings also correlate, indicating that higher magnetic field strength corresponds to lower heat transfer enhancement.

Fig. 13a, b, c, 14a, b, and 14c illustrate the impact of sine, square, and triangular wave frequencies and voltages on the average heat transfer across all flow rates at 60 Hz and 4 V for different Re. Notably, the results consistently indicate favorable heat transfer enhancement characteristics at 60 Hz and 4 V across various flow rates and Re for all waveform types compared to other frequencies and voltages at the same flow rate and Re. This observation underscores the significance of determining the optimal frequency and voltage for magnetic field application, correlating with an improved heat transfer coefficient across the tube.

The observed trend can be attributed to the behavior of magnetic properties within the fluid during flow and the resultant effects on

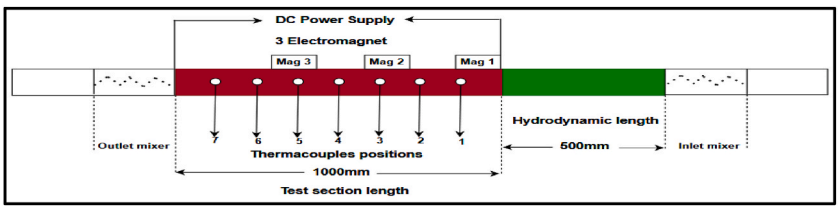

Fig. 10. Magnetic field positioning on the test section.

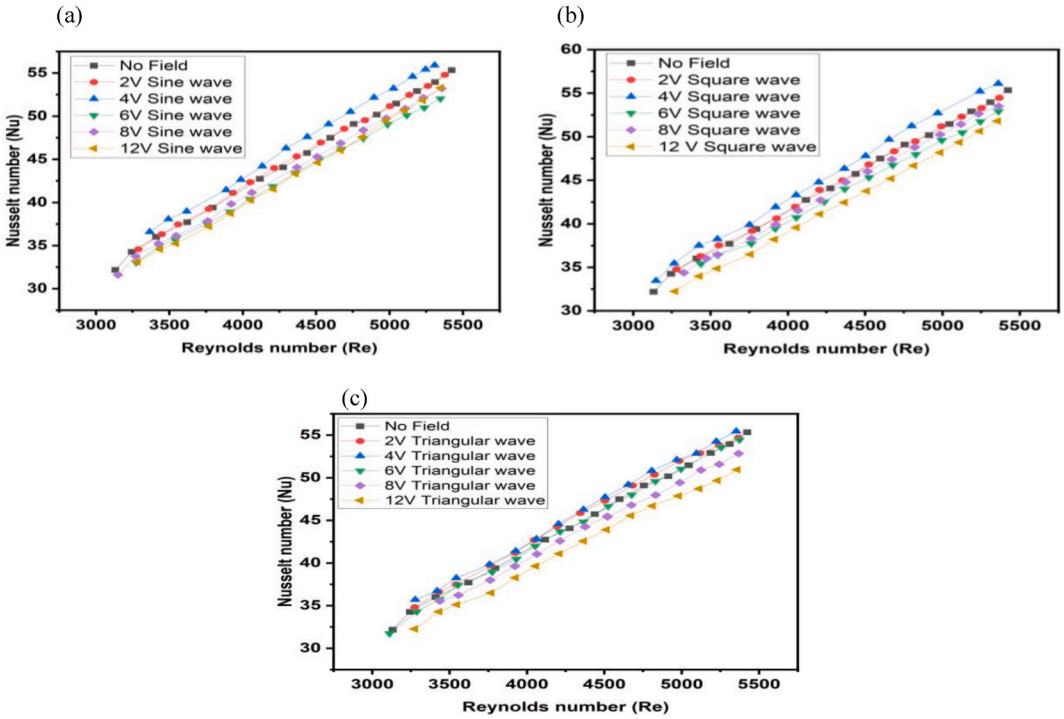

Fig. 11. (a) Voltage enhancement optimization Analysis on Sine waves (b) Voltage enhancement optimization analysis on square waves (c) Voltage enhancement optimization analysis on triangular waves.

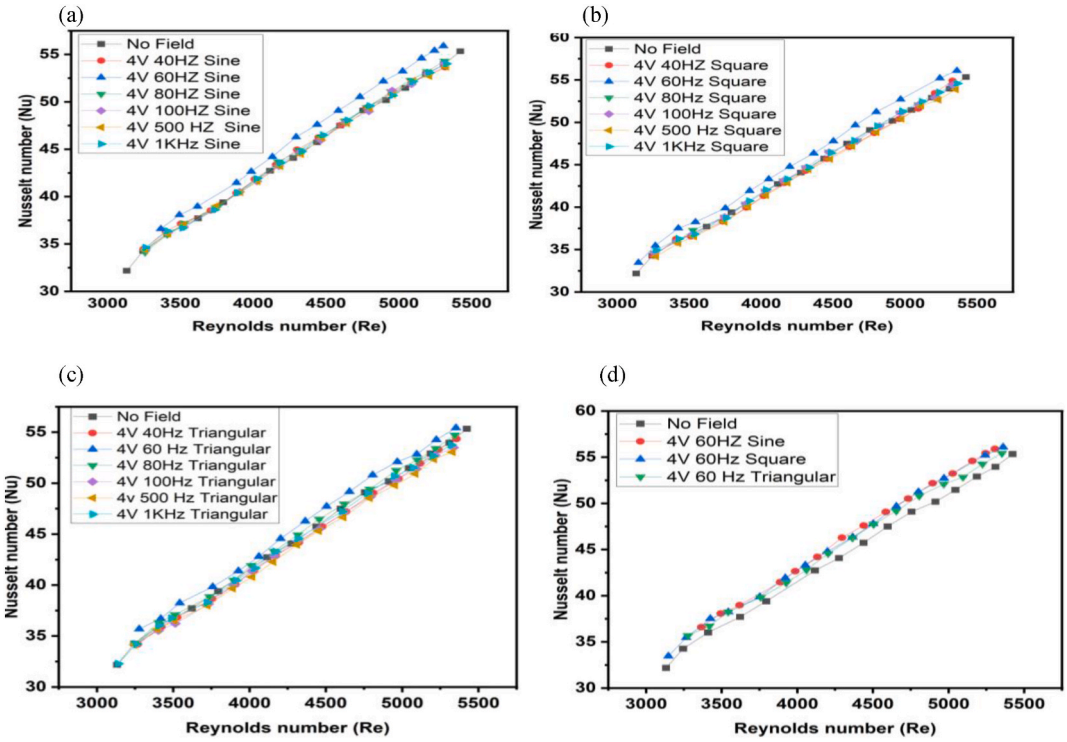

Fig. 12. (a): Frequency enhancement optimization: 4-V analysis on sine waves (b) Frequency enhancement optimization: 4-V analysis on square waves (c) Frequency enhancement optimization: 4-V analysis on triangular waves (d) Comparative analysis of frequency enhancement optimization at 4 V using sine waves, square waves, and triangular waves.

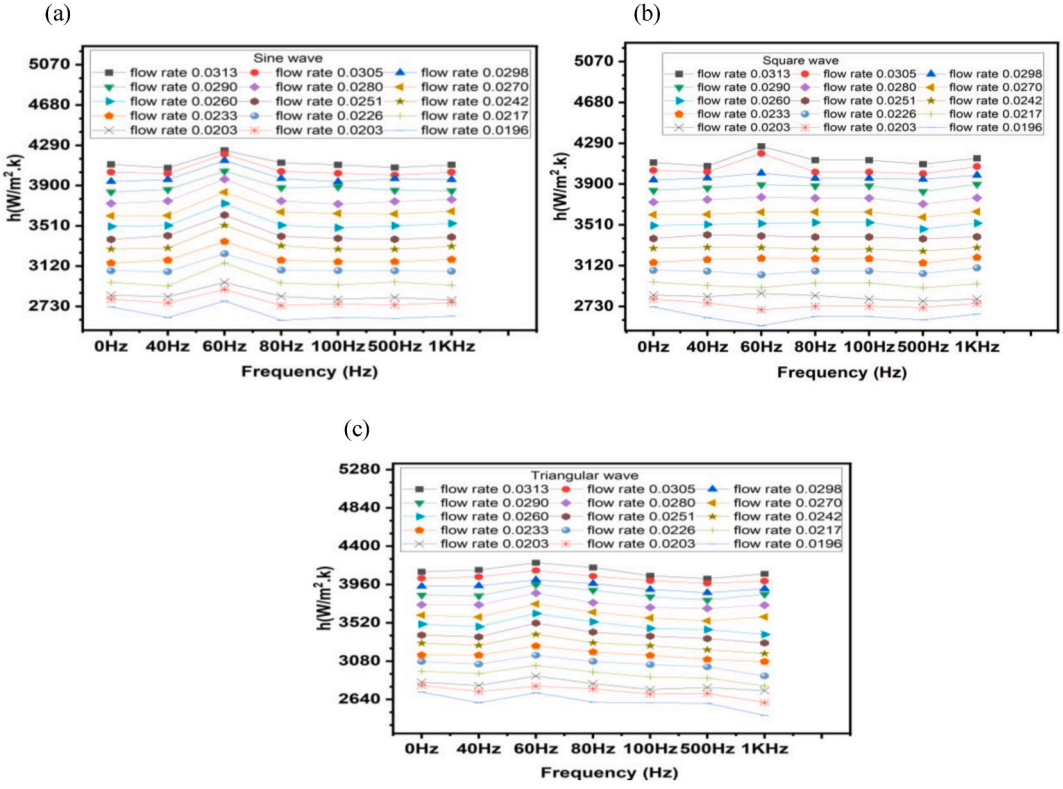

Fig. 13. (a) The influence sine waves frequency on average heat transfer (b) The influence square waves frequency on the average heat transfer (c) The influence triangular waves frequency on the average heat transfer.

nanoparticle dispersion, viscosity reduction, and alignment with flow characteristics. The magnetic properties are effectively suspended within the fluid at the optimal frequency and voltage, facilitating enhanced heat transfer rates. The enhancement of heat transfer at higher flow rates aligns with the findings of Heidari et al. (2021) [42], who noted that increasing the Reynolds number and solid volume fraction while decreasing the stairway aspect ratio enhances the average Nusselt number, indicating improved heat transfer efficiency. However, an increase in frequency and voltage leads to a stronger magnetic field, which may cause the fluid's magnetic properties to be attracted to the tube wall during flow, consequently reducing the heat transfer rate. In conclusion, determining the optimum magnetic field parameters is crucial for all pipe sizes and hybrid magnetic fluids to achieve improved heat transfer rates. This emphasizes the importance of carefully optimizing magnetic field conditions to maximize heat transfer efficiency in fluid flow systems.

The findings from Fig. 15a and b, and **c** collectively reveal a consistent pattern of heightened heat enhancement when sine wave, square wave, and triangular wave magnetic fields are introduced at varying volume fractions (0.1%, 0.05%, 0.025%, 0.0125%, and 0.00625%), as opposed to conditions without a magnetic field at the same volume fractions. This indicates a substantial influence of the magnetic field waves on improving fluid flow characteristics. Particularly noteworthy is the observable increase in heat enhancement, even at lower volume fractions such as 0.0125% and 0.00625%, with 0.0125% exhibiting the highest enhancement across the three waves. This suggests a distinct sensitivity of the field to wave concentrations. Furthermore, the comparison with DIW underscores that all concentrations, with and without a magnetic field, exhibit higher heat enhancement compared to DIW alone. This consistent trend implies that the introduction of magnetic waves, even at minimal concentrations, significantly contributes to augmenting fluid flow dynamics.

Fig. 16 and Table 5 provides a detailed comparison of the percentage enhancement of heat transfer using Fe_3O_4/TiO_2 nanofluids under the influence of magnetic field waves provides significant insights into optimizing thermal performance across various volume fractions. At a volume fraction of 0.1%, the heat transfer enhancement without a magnetic field was 16.5 %. However, the application of magnetic field waves resulted in slight reductions: 15.3% with sine waves (a 7.27% decrease), 13.26% with square waves (a 19.64% decrease), and 12.59% with triangular waves (a 23.70% decrease). This reduction might be due to the increased hydraulic resistance and disrupted fluid flow caused by the higher nanoparticle concentration.

In contrast, at a volume fraction of 0.05%, the magnetic field waves significantly improved the heat transfer enhancement compared to no magnetic field, which was 19.6%. With sine waves, the enhancement increased to 20.92% (a 6.73% increase), with square waves to 21.3% (an 8.67% increase), and with triangular waves to 21.34% (an 8.88% increase). This indicates that at medium concentrations, the magnetic field waves help align the nanoparticles and reduce thermal resistance, optimizing heat transfer.

For the 0.025% volume fraction, the enhancement without a magnetic field was 21%. The application of magnetic field waves

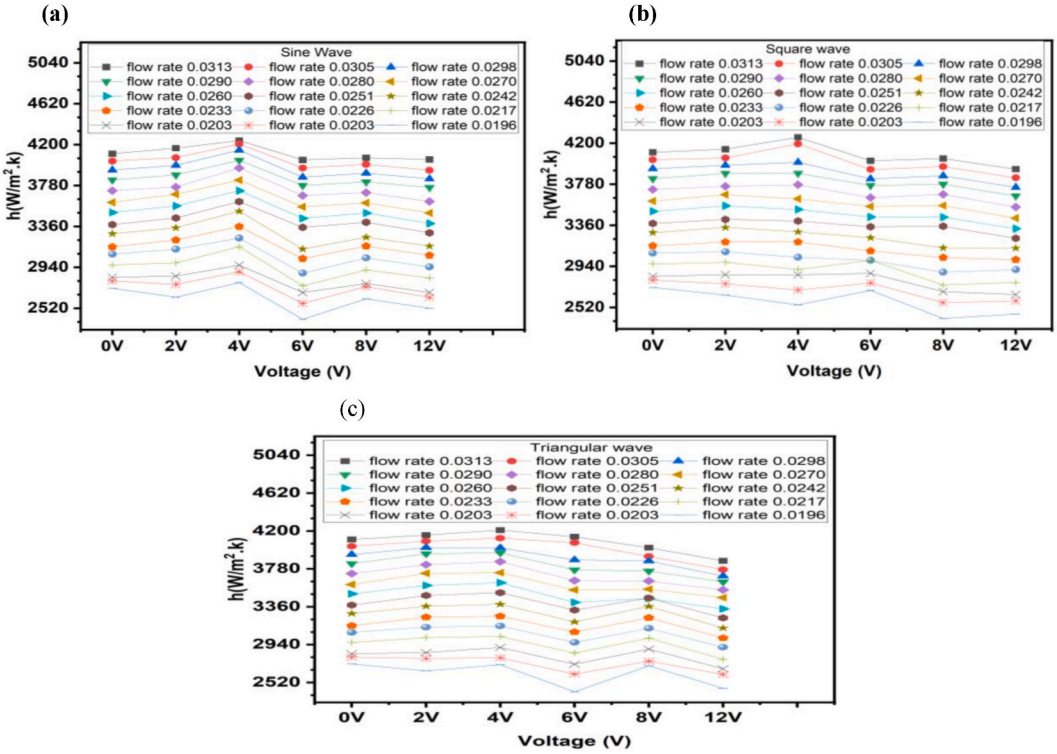

Fig. 14. (a) The influence sine waves frequency on average heat transfer (b) The influence square waves voltage on the average heat transfer. (c) The influence triangular waves voltage on the average heat transfer.

resulted in further improvements: 22.07% with sine waves (a 5.10% increase), 22.3% with square waves (a 6.19% increase), and 21.32% with triangular waves (a 1.52% increase). The square wave showed the highest enhancement, suggesting that at this concentration, the magnetic field enhances nanoparticle dispersion and alignment effectively.

The most significant enhancements were observed at lower volume fractions. At 0.0125%, the enhancement without a magnetic field was 26.5%, which increased to 27.87% with sine waves (a 5.17% increase), 28.21% with square waves (a 6.45% increase), and 26.74% with triangular waves (a 0.91% increase). This concentration shows the highest overall enhancements with magnetic waves, particularly with the square wave, indicating an optimal balance between nanoparticle concentration and magnetic field influence.

Finally, at a volume fraction of 0.0065%, the enhancement without a magnetic field was 22%. With the application of magnetic field waves, the enhancement increased to 22.24% with sine waves (a 1.09% increase), 22.3% with square waves (a 1.36% increase), and 24.49% with triangular waves (an 11.32% increase). The triangular wave showed a significant improvement, highlighting its effectiveness at low concentrations. The magnetic field likely aids in maintaining nanoparticle dispersion, enhancing thermal performance.

In summary, the application of magnetic field waves, particularly square and triangular waves, significantly enhances the heat transfer performance of Fe_3O_4/TiO_2 nanofluids, especially at lower to medium volume fractions. These findings emphasize the importance of optimizing both nanoparticle concentration and magnetic field parameters to achieve superior thermal efficiency in heat transfer applications.

Fig. 17a and b, and **c** present a comprehensive effect of volume fractions and comparison of the mean heat transfer coefficient (h_{avg}) for $Fe_3O_4/Ti\ O_2$ nanofluid under different magnetic field waveforms: sine, square, and triangular, respectively. The comparison includes a control condition without a magnetic field and DIW for reference. Observing the trend across various volume fractions of the nanofluid, there's a consistent decrease in the mean heat transfer coefficient with increasing volume fraction, indicating the influence of nanoparticle concentration on heat transfer enhancement. Analyzing the data also reveals the impact of the magnetic field on heat transfer efficiency, as evidenced by comparisons between mean heat transfer coefficients with and without a magnetic field at each volume fraction. Additionally, comparing the nanofluid's mean heat transfer coefficient to that of DIW provides valuable insights into its relative effectiveness in enhancing heat transfer. These findings underscore the intricate relationship between flow rate, volume fraction, magnetic field waveform, and heat transfer coefficient, offering valuable guidance for optimizing heat transfer in practical applications.

3.4. Percentage pressure drop as a function of flow rate for various volume fractions

Fig. 18a and b, and c illustrate the percentage pressure drop as a function of flow rate for various volume fractions under the

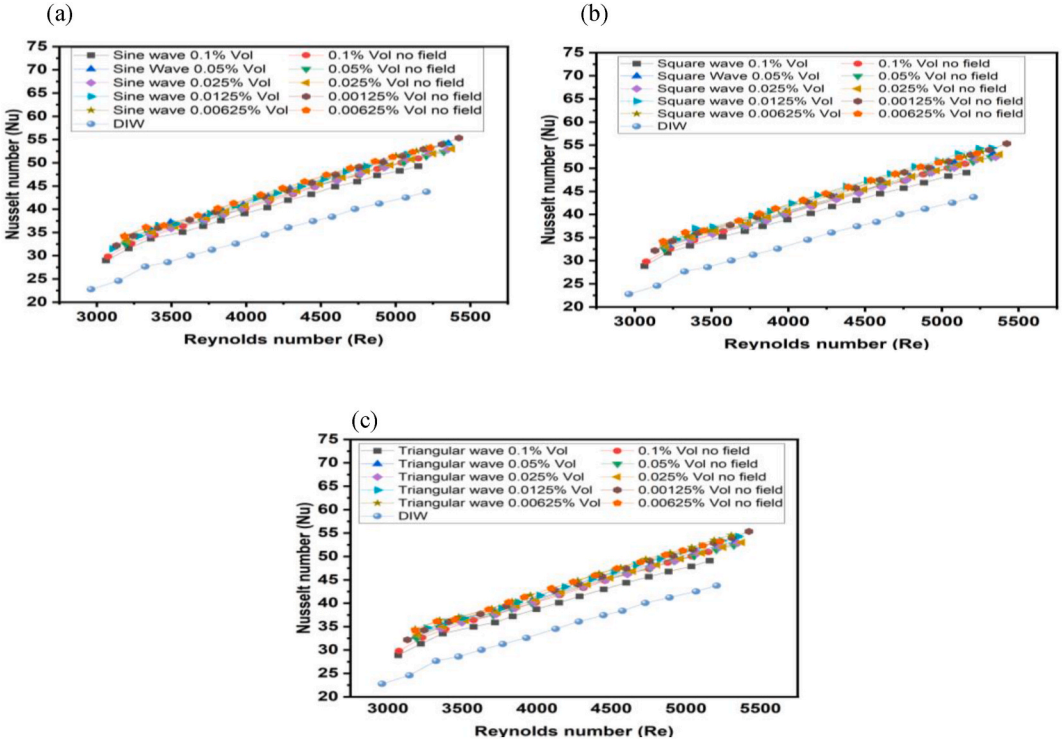

Fig. 15. (a) Enhancement of heat transfer with magnetic field sine waves at various volume fractions
(b) Enhancement of heat transfer with magnetic field square waves at various volume fractions
(c) Enhancement of heat transfer with magnetic field triangular waves at various volume fractions.

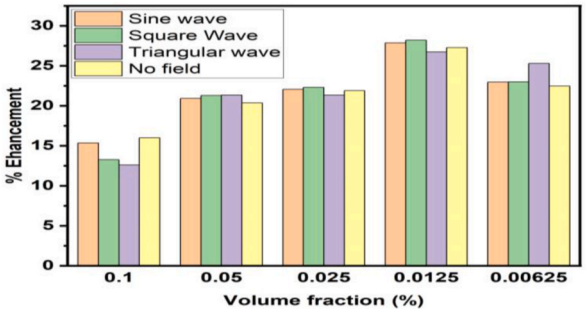

Fig. 16. Comparative analysis of heat transfer enhancement with different waveforms at varied volume fractions.

Table 5
Comparison of the percentage enhancement of heat transfer using Fe_3O_4/TiO_2 nanofluids under the influence of magnetic field waves.

% Volume fraction	% Enhancement with magnetic field	% Enhancement Sine waves	% Different from without magnetic field sine waves	% Enhancement Square waves	% Different from without magnetic field square waves	% Enhancement Triangular waves	% Different from without magnetic field Triangular waves
0.1	16.5	15.3	−7.27	13.26	−19.64	12.59	−23.64
0.05	19.6	20.92	6.73	21.3	8.67	21.34	8.87
0.025	21	22.07	5.10	22.3	6.19	21.32	1.5
0.0125	26.5	27.87	5.17	28.21	6.45	26.74	0.95
0.0065	22	22.24	1.09	22.3	1.36	24.49	11.32

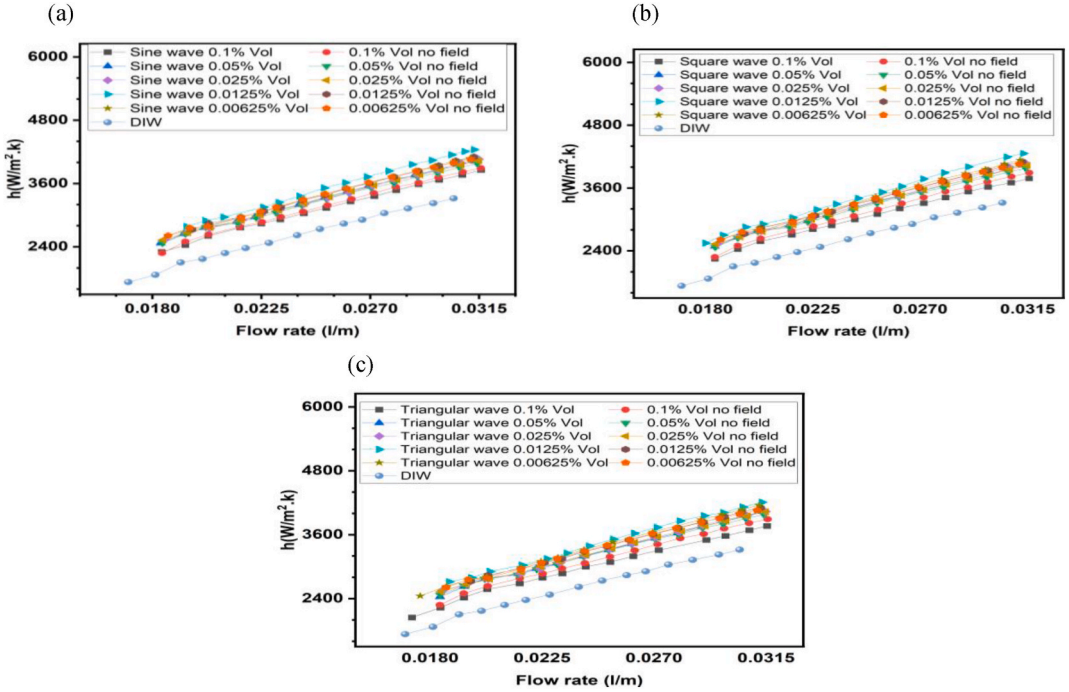

Fig. 17. (a) Effect of volumetric fractions, comparison of mean heat transfer coefficient for Fe_3O_4/Ti O_2 nanofluid under sine wave and flow rates, including no magnetic condition (b) Effect of volumetric fractions, comparison of mean heat transfer coefficient for Fe_3O_4/Ti O_2 nanofluid under square wave and flow rates, including no magnetic condition (c) Effect of volumetric fractions, comparison of mean heat transfer coefficient for Fe_3O_4/Ti O_2 nanofluid under triangular wave and flow rates, including no magnetic condition.

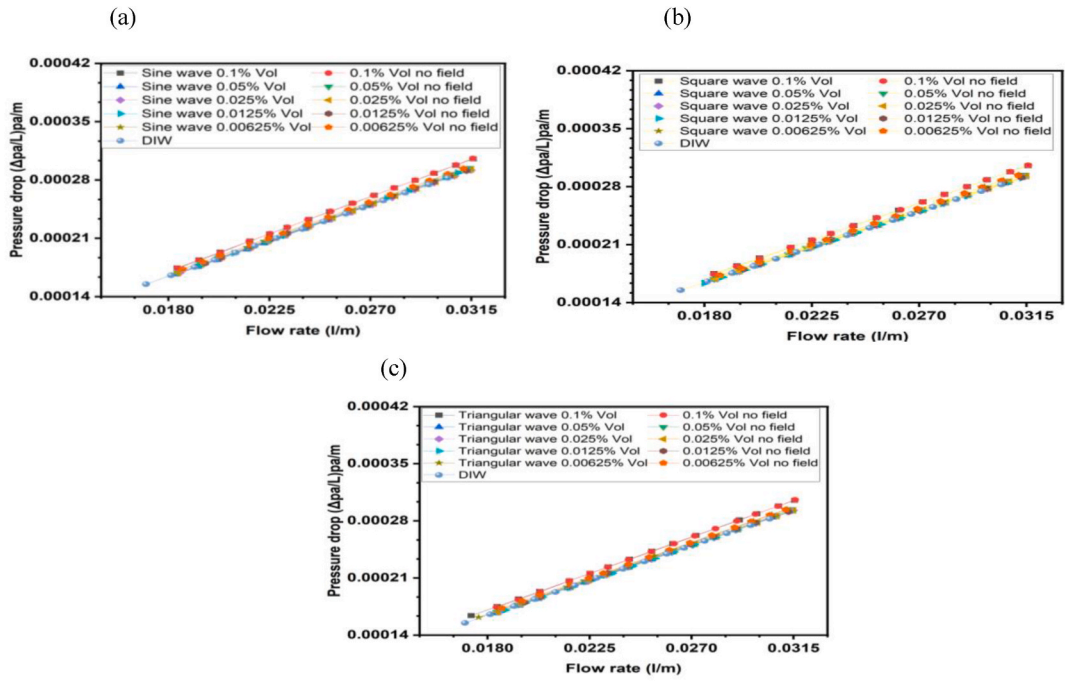

Fig. 18. (a) Effect of volumetric fractions and magnetic field sine wave on pressure drop in Fe_3O_4/Ti O_2 nanofluids across different flow rates (b) Effect of volumetric fractions and magnetic field square wave on pressure drop in Fe_3O_4/Ti O_2 nanofluids across different flow rates (c) Effect of volumetric fractions and magnetic field triangular wave on pressure drop in Fe_3O_4/Ti O_2 nanofluids across different flow rates.

Table 6
Percentage pressure drop across different magnetic waveforms and volume fractions in MHNFs nanofluids.

% Volume fraction	% Pressure drop with no magnetic field	% Pressure drop with Sine waves	% Pressure drop with Square waves	% Pressure drop with Triangular waves
0.1	3.69	3.73	3.67	3.64
0.05	3.44	3.42	3.21	3.40
0.025	3.23	3.12	3.06	3.08
0.0125	2.76	2.75	2.74	2.74
0.0065	2.3	2.22	2.15	2.13

influence of magnetic waves, specifically sine, square, and triangular waves. From Table 6, it is evident that higher volume fractions, such as 0.1%, correspond to increased pressure drops across all wave types: Sine Waves (3.73%), Square Waves (3.67%), and Triangular Waves (3.64%). This indicates greater resistance to flow, likely due to enhanced nanoparticle obstruction influenced by magnetic field-induced turbulence, which is potentially linked to fluid viscosity effects. Conversely, lower volume fractions (e.g., 0.0065% and 0.0125%) exhibit reduced pressure drops, suggesting smoother flow and minimized energy losses. This facilitates more efficient heat transfer, reducing dissipation as heat due to fluid friction and enhancing overall heat transfer properties.

The impact of magnetic fields on pressure drop varies with wave type. Sine Waves show modest variations in pressure drop, potentially influenced by alternating magnetic fields affecting nanoparticle orientation or movement differently. Square Waves exhibit a more pronounced decrease in pressure drop at lower volume fractions, indicating improved alignment or reduced resistance due to their specific waveform characteristics. Triangular Waves generally mirror Square Waves in trends, suggesting similar effects of magnetic field-induced turbulence and particle alignment.

Several factors contribute to these pressure drop effects, including particle alignment and turbulence induced by magnetic fields, flow obstruction due to higher volume fractions, and energy dissipation mechanisms. Magnetic fields can either increase or decrease turbulence, thereby affecting pressure drops differently depending on fluid viscosity and flow dynamics. Lower pressure drops typically indicate smoother flow conditions and better energy efficiency, which are crucial for optimizing heat transfer processes in nanofluids under varying magnetic field conditions.

Moreover, the relationship between pressure drops and flow rate across all concentrations exhibits a linear decrease. Interestingly, this linear trend closely resembles the behavior observed in DIW at lower concentrations (0.00625 and 0.01255 % vol), suggesting that while flow rate remains the primary determinant, nanoparticle concentration exacerbates the pressure drop. This observation aligns with prior research findings by Emad et al. [29], Ashjaee et al. [43] and Sundar [44]. These findings show the intricate interplay between magnetic field effects, fluid dynamics, and thermal efficiency in advanced heat transfer applications, highlighting the need for a comprehensive understanding and control of these factors for enhanced MHNFs nanofluid-based heat management systems.

3.4.1. Hypothesis for the varied impact of different magnetic waveforms on pressure drop and comparative analysis

A plausible hypothesis for the varied impact of different magnetic waveforms on pressure drop is that the nature of the magnetic field influences the alignment and interaction of nanoparticles within the fluid. For instance, sine waves produce a smooth, continuous variation in the magnetic field, potentially allowing for gradual realignment of nanoparticles, which might reduce sudden changes in flow resistance. On the other hand, with their abrupt transitions, square waves might cause more significant disturbances in the nanoparticle alignment, leading to either improved or worsened flow conditions depending on the volume fraction. Triangular waves, having characteristics of both sine and square waves, could produce intermediate effects. These findings are consistent with previous studies. For example, Emad et al. [29], noted that magnetic fields could both enhance and disrupt fluid flow depending on the waveform characteristics. Ashjaee et al. [43] found that magnetic field-induced turbulence could either increase or decrease flow resistance, aligning with this study's observed pressure drop trends. Sundar [44] also reported the dual effects of magnetic fields on nanoparticle alignment and fluid dynamics.

These intricate interactions between magnetic field effects, fluid dynamics, and thermal efficiency underscore the need to comprehensively understand and control these factors in MHNFs nanofluid-based heat management systems. By leveraging the unique properties of different magnetic waveforms, it is possible to optimize pressure drops and enhance heat transfer efficiency in advanced thermal systems.

3.5. Effect of magnetic waveforms on thermal efficiency on MHNFs

The assessment of thermal efficiency is crucial for evaluating Fe_3O_4/Ti O_2 nanofluids across various waveforms in heat transfer systems. It gauges energy conversion effectiveness, aiding in optimizing heat transfer processes under different waveform dynamics. Defined by Equation (18) [45], it serves as a pivotal metric guiding engineering decisions.

$$\eta = \frac{\frac{h_{avg,bf}}{h_{avg,nf}}}{\frac{\Delta P_{nf}}{\Delta P_{bf}}} \tag{18}$$

In Fig. 19a, b, and c, and Table 7, the analysis of Fe_3O_4/TiO_2 nanofluids under varying magnetic field strengths and waveforms revealed significant impacts on thermal efficiency at the lowest flow rate. For a 0.1% volume fraction, introducing sine waves led to a thermal

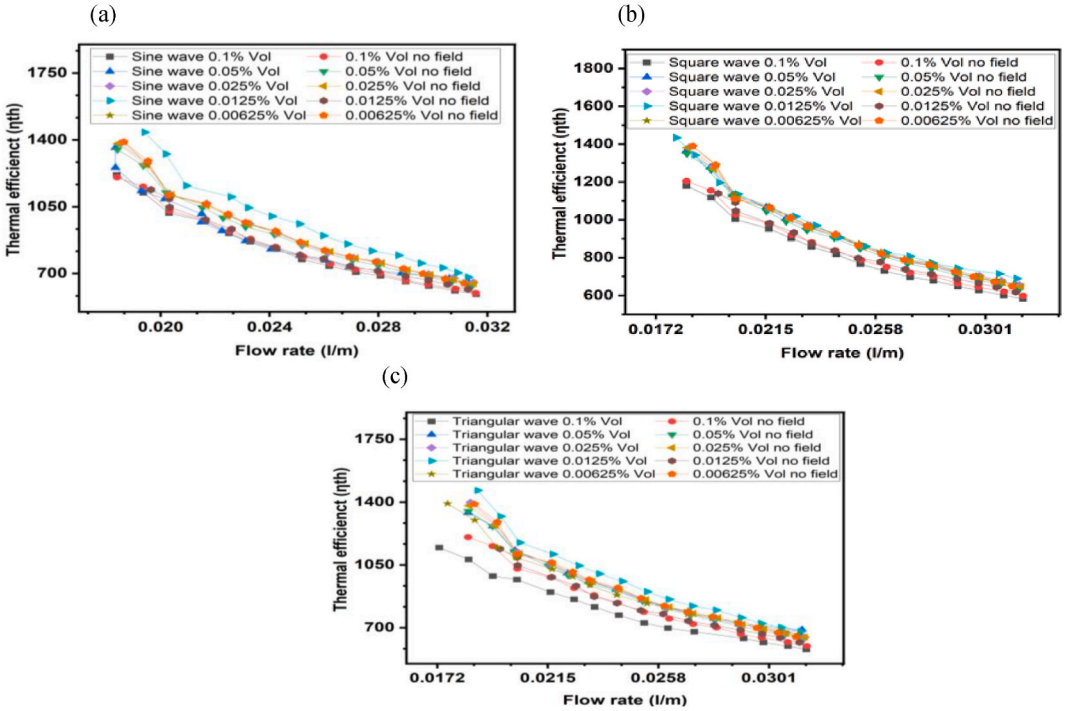

Fig. 19. (a) Effect of magnetic field sine waveform and volume fractions on thermal efficiency of $Fe_3O_4/Ti\ O_2$ nanofluids across various flow rates (b) Effect of magnetic field square waveform and volume fractions on thermal efficiency of $Fe_3O_4/Ti\ O_2$ nanofluids across various flow rates (C) Effect of magnetic field triangular waveform and volume fractions on thermal efficiency of $Fe_3O_4/Ti\ O_2$ nanofluids across various flow rate.

Table 7
Thermal Efficiency of Fe_3O_4/TiO_2 Nanofluids at Various Volume Fractions Under Different Magnetic Field Waveforms and No Magnetic Field Conditions at the lowest flow rate.

% Volume fraction	Thermal efficiency no magnetic field	Thermal efficiency with Sine waves	Thermal efficiency with Square waves	Thermal efficiency Triangular waves
0.1	1204	1215	1179	1146
0.05	1349	1359	1363	1340
0.025	1380	1382	1383	1397
0.0125	1439	1440	1434	1464
0.0065	1389	1388	1388	1392

efficiency enhancement of 0.91% compared to the no magnetic field condition. In comparison, square and triangular waves decreased by 2.08% and 4.82%, respectively. At a 0.05% volume fraction, sine waves improved thermal efficiency by 0.74%, square waves by 1.04%, and triangular waves saw a slight reduction of 0.67%. Enhancements were more modest for the 0.025% volume fraction, with sine waves increasing efficiency by 0.14%, square waves by 0.22%, and triangular waves showing the highest increase at 1.23%. At a

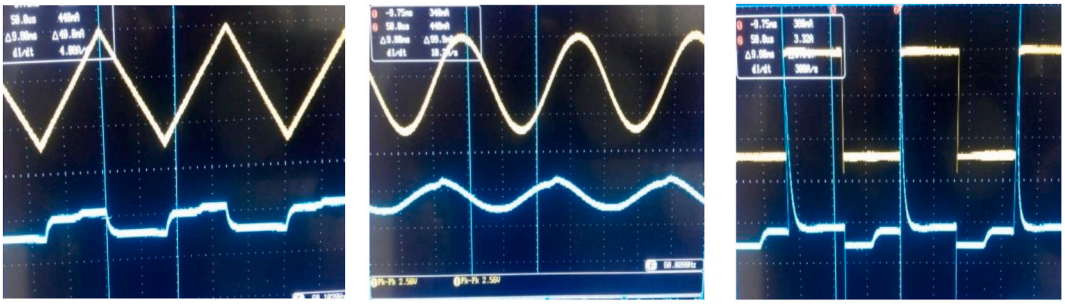

Fig. 20. The pictorial capture of each wave type used (a) Triangle wave, (b) Sine wave and (c) Square wave.

0.0125% volume fraction, sine waves provided a minimal improvement of 0.07%, square waves decreased efficiency by 0.35%, while triangular waves offered a notable enhancement of 1.74%. Finally, for the 0.0065% volume fraction, sine and square waves both led to a minor decrease in thermal efficiency by 0.07%, whereas triangular waves provided a slight increase of 0.22%.

The optimum thermal efficiency across all waveforms and volume fractions was observed at the 0.0125% volume fraction with triangular waves, achieving an enhancement of 1.74% over no magnetic field. The trend is clearly shown, as the flow rate decreases, the thermal efficiency increases. This trend is consistent across all volume fractions and waveforms.

This discrepancy is primarily attributed to the higher concentration of solid particles in these mixtures, disrupting fluid flow and increasing thermal resistance, thereby lowering thermal efficiency. A noticeable inverse correlation is observed as particle concentration decreases from 0.1% Vol. to 0.05% Vol., suggesting a trade-off between concentration and thermal performance. Lower concentrations offer more favorable thermal efficiency outcomes, possibly due to improved uniformity in nanoparticle dispersion, which enhances heat transfer. Conversely, higher concentrations may experience particle aggregation or uneven distribution, hindering effective heat transfer. These findings highlight the nuanced effects of magnetic field waveforms on thermal efficiency across different nanoparticle concentrations at the lowest flow rate, underscoring the importance of optimizing these parameters for enhanced heat transfer performance in MHNFs nanofluid applications.

Fig. 20 shows the pictorial capture of each wave type used for this study.

4. Conclusion

Utilizing a magnetic field to influence convective flow in ferrofluids has emerged as an effective technique for enhancing heat transfer in thermal systems, particularly in straight tubes. This study investigates the heat transfer properties of Fe_3O_4/Ti O_2 nanofluids within a heated copper tube under varied magnetic field strengths and waveforms. The following are the main findings:

- Magnetic field strengths and waveforms significantly influence heat transfer properties in Fe_3O_4/Ti O_2 nanofluids, with optimal conditions identified at 4 V and 60 Hz across all waveforms.
- Higher magnetic field frequencies and voltages decrease heat transfer rates due to increased magnetic field intensity.
- Pressure drop variations across waveforms suggest altered nanoparticle alignment and turbulence levels, affecting fluid flow dynamics and viscosity.
- Higher nanoparticle volume fractions (0.1%) increase flow resistance and reduce thermal efficiency, while lower concentrations enhance thermal performance by improving nanoparticle dispersion.
- Magnetic field application generally attenuates heat transfer enhancement: at 0.1 % volume fraction, enhancements decrease to 15.3% (sine), 13.26% (square), and 12.59% (triangular).
- Lower volume fractions (0.05%–0.0065%) demonstrate improved heat transfer enhancements with magnetic fields, exceeding performance without magnetic fields across all waveforms.
- Further research could explore additional factors such as particle size and fluid properties to refine understanding and improve the efficiency of nanofluid-based thermal management systems.

These findings highlight the intricate relationship between magnetic field parameters, nanoparticle behavior, and thermal performance in nanofluid applications, offering insights for optimizing heat transfer processes.

CRediT authorship contribution statement

Victor O. Adogbeji: Writing – original draft, Investigation, Formal analysis, Data curation, Conceptualization. **Mohsen Sharifpur:** Writing – review & editing, Supervision, Resources, Methodology, Funding acquisition. **Josua P. Meyer:** Writing – review & editing, Validation, Supervision, Methodology.

Data availability

Upon request, the data can be provided. approach, necessitating further research for comprehensive understanding and optimization in diverse practical applications.

Declaration of competing interest

The authors affirm that they do not have any known monetary interests or personal relationships that might be perceived as influencing the work presented in this paper.

Abbreviations

AC	Alternating
ACMF	Alternating current magnetic field
Al	Aluminium nanoparticles
AL_2O_3	Aluminium oxide nanoparticles

Au	Gold nanoparticles
C_p	Specific heat transfer
Co_2O_3	Cobalt (III) oxide nanoparticles
Cu	Copper nanoparticles
CuO	Copper oxide nanoparticles
CHT	Convective heat transfer
CNTs	Carbon nanotubes
DC	Direct current
Di	Internal diameter of the tube
DIW	Deionized water
DW	Distilled water
EG	Ethylene glycol
Fe_2O_3	Iron (III) oxide nanoparticles
Fe_3O_4	Iron (IV) oxide nanoparticles
G	Gauss
GA	Gum Arabic
GMO	Graphene magnetite oxide
I	Current (Ampere)
$\dot{m}$	Mass flow rate
MF	Magnetic fields
MHNFs	Magnetic hybrid nanofluids
MNFs	Magnetic nanofluids
MNPs	Magnetic nanoparticles
MWCNT	Multiwalled carbon nanoparticle
mT	Millitesla
mV	Millivolts
$\dot{q}$	Heat flux, W /m^2
SF	Sedimentation Factor
SiO_2	Silicon oxide nanoparticles
STDEV	Standard deviation
TEM	Transmission electron microscopy
Ti O_2	Titanium oxide nanoparticles
UV–Vis	Ultra Violet-Visible
V	Voltage
x/d	Axial distance

Greek symbols

φ	mass ratio of nanofluids
Φ	Volume concentration (vol%)
μ	Viscosity (mPas)
κ	Thermal conductivity (W/K-1)
σ	Electrical conductivity (mS/cm −1)
η	Thermal efficiency

Subscripts

A_o	Initial Absorbance
A_t	Final Absorbance
avg	Average
u_B	Bias error
u_p	Precision error
bf	base fluid
C_p	Specific heat capacity of particles (J/kg-K)
C_{pnf}	specific heat capacity of nanofluids (J/kg-K)
C_{pbf}	specific heat capacity of base fluids (J/kg-K)
C_{pnp}	specific heat capacity of nanoparticles (J/kg-K)
ρ_{nf}	Densities of the nanofluid (Kg /m^3)
ρ_{bf}	Density of base fluid (Kg /m^3)
$\varphi\rho_{np}$	Density of nanoparticles (Kg /m^3)
h_{avg}	Average heat transfer coefficient (W /m^2-K)
T_O	outlet °C

T_i inlet °C
t_w wall temperature °C
t_b bulk temperature °C
n_f nanofluid
n_p nanoparticles

Dimensionless Numbers
Nu Nusselt number
Re Reynold number
Pr Prandtl number

Data availability

Data will be made available on request.

References

[1] A.S. John, B. Mahanthesh, I.V. Shevchuk, Study of nanofluid flow and heat transfer in a stationary cone-disk system, Therm. Sci. Eng. Prog. 46 (June) (2023) 102173, https://doi.org/10.1016/j.tsep.2023.102173.
[2] E.O. Atofarati, M. Sharifpur, J. Meyer, Hydrodynamic effects of hybrid nanofluid jet on the heat transfer augmentation, Case Stud. Therm. Eng. 51 (Nov. 2023) 103536, https://doi.org/10.1016/J.CSITE.2023.103536.
[3] M. Bezaatpour, H. Rostamzadeh, J. Bezaatpour, Hybridization of rotary absorber tube and magnetic field inducer with nanofluid for performance enhancement of parabolic trough solar collector, J. Clean. Prod. 283 (2021) 124565, https://doi.org/10.1016/j.jclepro.2020.124565.
[4] F. Selimefendigil, H.F. Oztop, A.J. Chamkha, Jet impingement heat transfer of confined single and double jets with non-Newtonian power law nanofluid under the inclined magnetic field effects for a partly curved heated wall, Sustain. Times 13 (9) (2021), https://doi.org/10.3390/su13095086.
[5] S.Z. Heris, F. Mohammadpur, O. Mahian, A.Z. Sahin, Experimental study of two phase closed thermosyphon using cuo/water nanofluid in the presence of electric field, Exp. Heat Tran. 28 (4) (2015) 328–343, https://doi.org/10.1080/08916152.2014.883448. Taylor & Francis.
[6] E. Raki, M. Afrand, A. Abdollahi, Influence of magnetic field on boiling heat transfer coefficient of a magnetic nanofluid consisting of cobalt oxide and deionized water in nucleate regime: an experimental study, Int. J. Heat Mass Tran. 165 (2021) 120669, https://doi.org/10.1016/j.ijheatmasstransfer.2020.120669.
[7] P. Ganesh Kumar, V.S. Vigneswaran, V. Sivalingam, R. Velraj, S.C. Kim, V. Ramkumar, Enhancing heat transfer performance of automotive radiator with H2O/ activated carbon nanofluids, J. Mol. Liq. 371 (2023) 121153, https://doi.org/10.1016/j.molliq.2022.121153.
[8] I.U. Ibrahim, M. Sharifpur, J.P. Meyer, Experimental investigations of particle sizes effects on exergy and entropy characteristics of AL2O3 - MWCNT hybrid nanofluid along the transitional flow regime, Case Stud. Therm. Eng. 51 (Nov. 2023) 103575, https://doi.org/10.1016/j.csite.2023.103575.
[9] A. Shahsavar, et al., Experimental investigation of the effect of mechanical vibration and rotating magnetic field on the hydrothermal performance of water-Fe3O4 ferrofluid inside a rifled tube, J. Magn. Magn Mater. 572 (November 2022) (2023), https://doi.org/10.1016/j.jmmm.2023.170586.
[10] S. Wu, C. Rincon Ortiz, Experimental investigation of the effect of magnetic field on vapour absorption with LiBr–H2O nanofluid, Energy 193 (2020) 1–9, https://doi.org/10.1016/j.energy.2019.116640.
[11] V. Baldin, L.R.R. da Silva, A.R. Machado, C.F. Houck, State of the art of biodegradable nanofluids application in machining processes, Korean Society for Precision Engineering 10 (5) (2023), https://doi.org/10.1007/s40684-022-00486-0.
[12] M. Tekir, E. Taskesen, B. Aksu, E. Gedik, K. Arslan, Comparison of bi-directional multi-wave alternating magnetic field effect on ferromagnetic nanofluid flow in a circular pipe under laminar flow conditions, Appl. Therm. Eng. 179 (Oct) (2020), https://doi.org/10.1016/j.applthermaleng.2020.115624.
[13] M. Gürdal, E. Gürsoy, H.K. Pazarlıoğlu, K. Arslan, E. Gedik, An innovative approach of alternating magnetic field diversified with different wave types and magnet positions for ferrofluid flow in dimpled tube, J. Magn. Magn Mater. 581 (June) (2023), https://doi.org/10.1016/j.jmmm.2023.170975.
[14] A. Abadeh, M. Sardarabadi, M. Abedi, M. Pourramezan, M. Passandideh-Fard, M.J. Maghrebi, Experimental characterization of magnetic field effects on heat transfer coefficient and pressure drop for a ferrofluid flow in a circular tube, J. Mol. Liq. 299 (Feb) (2020), https://doi.org/10.1016/j.molliq.2019.112206.
[15] B. Sun, Y. Guo, D. Yang, H. Li, The effect of constant magnetic field on convective heat transfer of Fe3O4/water magnetic nanofluid in horizontal circular tubes, Appl. Therm. Eng. 171 (May 2020), https://doi.org/10.1016/j.applthermaleng.2020.114920.
[16] X. Zhang, Y. Zhang, Experimental study on enhanced heat transfer and flow performance of magnetic nanofluids under alternating magnetic field, Int. J. Therm. Sci. 164 (January) (2021) 106897, https://doi.org/10.1016/j.ijthermalsci.2021.106897.
[17] M. Goharkhah, A. Salarian, M. Ashjaee, M. Shahabadi, Convective heat transfer characteristics of magnetite nanofluid under the influence of constant and alternating magnetic field, Powder Technol. 274 (Apr. 2015) 258–267, https://doi.org/10.1016/j.powtec.2015.01.031.
[18] A.A. Karamallah, A. Habeeb Askar, L. Habeeb, The effect of magnetic field with nanofluid on heat transfer in a horizontal pipe investment cost analysis view project how to use engineering equation solver (EES): refrigeration and heat transfer applications view project the effect of magnetic field, Al-Khwarizmi Eng. J. 12 (3) (2016) 99–109.
[19] A. Lee, Y. Jeon, V. Chinnasamy, H. Cho, Investigation of forced convective heat transfer with magnetic field effect on water/ethylene glycol-cobalt zinc ferrite nanofluid, Int. Commun. Heat Mass Tran. 128 (October) (2021) 105647, https://doi.org/10.1016/j.icheatmasstransfer.2021.105647.
[20] A. Shahsavar, M. Saghafian, M.R. Salimpour, M.B. Shafii, Experimental investigation on laminar forced convective heat transfer of ferrofluid loaded with carbon nanotubes under constant and alternating magnetic fields, Exp. Therm. Fluid Sci. 76 (Sep. 2016) 1–11, https://doi.org/10.1016/j.expthermflusci.2016.03.010.
[21] M. Tekir, E. Taskesen, E. Gedik, K. Arslan, B. Aksu, Effect of constant magnetic field on Fe3O4-Cu/water hybrid nanofluid flow in a circular pipe, Heat Mass Transf. und Stoffuebertragung 58 (5) (May 2022) 707–717, https://doi.org/10.1007/s00231-021-03125-7.
[22] L. Shi, Y. Hu, Y. He, Magnetocontrollable convective heat transfer of nanofluid through a straight tube, Appl. Therm. Eng. 162 (Nov) (2019), https://doi.org/10.1016/j.applthermaleng.2019.114220.
[23] H. Talebi, M. H, V. Kalantar, Nazari, M.R. Kargarsharifabad, Experimental investigation of the forced convective heat transfer of hybrid Cu/Fe3O4 nanofluids, J. solid Fluid Mech. 8 (4) (2019) 229–238, https://doi.org/10.22044/jsfm.2019.7350.2687.
[24] M. Mehrali, et al., Heat transfer and entropy generation analysis of hybrid graphene/Fe3O4 ferro-nanofluid flow under the influence of a magnetic field, Powder Technol. 308 (Feb. 2017) 149–157, https://doi.org/10.1016/j.powtec.2016.12.024.
[25] S. Shyam, B. Mehta, P.K. Mondal, S. Wongwises, Investigation into the thermo-hydrodynamics of ferrofluid flow under the influence of constant and alternating magnetic field by InfraRed Thermography, Int. J. Heat Mass Tran. 135 (2019) 1233–1247, https://doi.org/10.1016/j.ijheatmasstransfer.2019.02.050.
[26] S.O. Giwa, M. Sharifpur, J.P. Meyer, Experimental study of thermo-convection performance of hybrid nanofluids of Al2O3-MWCNT/water in a differentially heated square cavity, Int. J. Heat Mass Tran. 148 (Feb) (2020), https://doi.org/10.1016/j.ijheatmasstransfer.2019.119072.

[27] B.C. Pak, Y.I. Cho, Hydrodynamic and heat transfer study of dispersed fluids with submicron metallic oxide particles, Exp. Heat Tran. 11 (2) (1998) 151–170, https://doi.org/10.1080/08916159808946559.
[28] V. Chinnasamy, J. Ham, H. Cho, Comparative investigation of convective heat transfer and pressure drop characteristics of MWCNT, Fe3O4, and MWCNT/Fe3O4 nanofluids, Case Stud. Therm. Eng. 47 (Jul) (2023), https://doi.org/10.1016/j.csite.2023.103095.
[29] E. Sadeghinezhad et al., "Experimental Study on Heat Transfer Augmentation of Graphene Based Ferrofluids in Presence of Magnetic Field", doi: 10.1016/j.applthermaleng.2016.11.199..
[30] A.J. Ghajar, L.M. Tam, Heat transfer measurements and correlations in the transition region for a circular tube with three different inlet configurations, Exp. Therm. Fluid Sci. 8 (1) (1994) 79–90, https://doi.org/10.1016/0894-1777(94)90075-2.
[31] J.A. Olivier, J.P. Meyer, Single-phase heat transfer and pressure drop of the cooling of water inside smooth tubes for transitional flow with different inlet geometries (rp-1280), HVAC R Res. 16 (4) (2010) 471–496, https://doi.org/10.1080/10789669.2010.10390916.
[32] P.F. Dunn, Measurement and Data Analysis for Engineering and Science, second ed., Taylor and Francis/CRC Press, 2010, pp. 1–7, c 2010 ISBN : 9781439825686," no. August 2009.
[33] S.O. Giwa, M. Sharifpur, M.H. Ahmadi, S.M. Sohel Murshed, J.P. Meyer, Experimental investigation on stability, viscosity, and electrical conductivity of water-based hybrid nanofluid of mwcnt-fe2o3, Nanomaterials 11 (1) (Jan. 2021) 1–19, https://doi.org/10.3390/nano11010136.
[34] S. Osman, M. Sharifpur, J.P. Meyer, Experimental investigation of convection heat transfer in the transition flow regime of aluminium oxide-water nanofluids in a rectangular channel, Int. J. Heat Mass Tran. 133 (Apr. 2019) 895–902, https://doi.org/10.1016/j.ijheatmasstransfer.2018.12.169.
[35] S. Suseel Jai Krishnan, M. Momin, C. Nwaokocha, M. Sharifpur, J.P. Meyer, An empirical study on the persuasive particle size effects over the multi-physical properties of monophase MWCNT-Al2O3 hybridized nanofluids, J. Mol. Liq. 361 (Sep) (2022), https://doi.org/10.1016/j.molliq.2022.119668.
[36] A. Arifutzzaman, A.F. Ismail, I.I. Yaacob, M.Z. Alam, A.A. Khan, Stability investigation of water based exfoliated graphene nanofluids, in: IOP Conference Series: Materials Science and Engineering, Institute of Physics Publishing, Mar. 2019, https://doi.org/10.1088/1757-899X/488/1/012002.
[37] S.S. Jyothirmayee, P. Baskar, T. Theres, K. Sabareesh, S. Das, S. Ramaprabhu, Investigation of structural stability, dispersion, viscosity, and conductive heat transfer properties of functionalized carbon nanotube based nanofluids, J. Phys. Chem. C 115 (2011) 16737–16744, https://doi.org/10.1021/jp201672p.
[38] A. Oraon, et al., Impact of magnetic field on the thermal properties of chemically synthesized Sm-Co nanoparticles based silicone oil nanofluid, J. Therm. Anal. Calorim. 147 (3) (2022) 1933–1943, https://doi.org/10.1007/s10973-021-10572-1.
[39] M. Zadkhast, D. Toghraie, A. Karimipour, Developing a new correlation to estimate the thermal conductivity of MWCNT-CuO/water hybrid nanofluid via an experimental investigation, J. Therm. Anal. Calorim. 129 (2) (Aug. 2017) 859–867, https://doi.org/10.1007/S10973-017-6213-8.
[40] R. Azizian, E. Doroodchi, T. McKrell, J. Buongiorno, L.W. Hu, B. Moghtaderi, Effect of magnetic field on laminar convective heat transfer of magnetite nanofluids, Int. J. Heat Mass Tran. 68 (2014) 94–109, https://doi.org/10.1016/j.ijheatmasstransfer.2013.09.011.
[41] N. Hatami, A. Kazemnejad Banari, A. Malekzadeh, A.R. Pouranfard, The effect of magnetic field on nanofluids heat transfer through a uniformly heated horizontal tube, Physics Letters, Section A: General, Atomic and Solid State Physics 381 (5) (Feb. 05, 2017) 510–515, https://doi.org/10.1016/j.physleta.2016.12.017. Elsevier B.V.
[42] H. Heidari, R. Mohebbi, A. Kazemi, Forced convection heat transfer of Ag-MgO/water micropolar hybrid nanofluid inside a stairway channel, Int. J. Mod. Phys. C 32 (11) (2021) 2021, https://doi.org/10.1142/S0129183121501473.
[43] M. Ashjaee, M. Goharkhah, L.A. Khadem, R. Ahmadi, Effect of magnetic field on the forced convection heat transfer and pressure drop of a magnetic nanofluid in a miniature heat sink, Heat Mass Transf. und Stoffuebertragung 51 (7) (Jul. 2015) 953–964, https://doi.org/10.1007/s00231-014-1467-1.
[44] L.S. Sundar, M.K. Singh, A.C.M. Sousa, Enhanced heat transfer and friction factor of MWCNT-Fe3O4/water hybrid nanofluids, Int. Commun. Heat Mass Tran. 52 (Mar. 2014) 73–83, https://doi.org/10.1016/j.icheatmasstransfer.2014.01.012.
[45] M. Goharkhah, M. Ashjaee, M. Shahabadi, Experimental investigation on convective heat transfer and hydrodynamic characteristics of magnetite nanofluid under the influence of an alternating magnetic field, Int. J. Therm. Sci. 99 (Jan. 2016) 113–124, https://doi.org/10.1016/j.ijthermalsci.2015.08.008.